

AN ABSTRACT OF THE THESIS OF

Cheng Zeng for the degree of Master of Science in Chemical Engineering presented on November 30, 2018.

Title: Formation of $\text{Cu}_2\text{ZnSnS}_4$ Thin Films via Reactive Sintering of Binary Metal-Sulfide Nanoparticles Using Intense Pulsed Light

Abstract approved: _____

Chih-hung Chang

Copper zinc tin sulfide (CZTS) is a potential solar material for thin film solar cells according to its suitable band gap in the visible light range, high absorption coefficient, low toxicity, good photostability and relative earth abundance of component elements. However, the production cost of this solar thin film material is dominated by the vacuum-based thin film deposition techniques and the production throughput is limited by the long-term heating processes.

In order to improve the process a high output and short-term process, solution-based thin film deposition methods such as spin coating and inkjet printing have been studied to build the thin film while several sintering methods including intense pulsed light (IPL) sintering, UV curing, and xenon sintering have been studied to replace the more traditional

thermal sintering process. Different measurements including X-ray diffraction, Raman spectroscopy, scanning electron microscope, transmission electron microscopy and Hall effect measurement have been used to characterize the structures and properties of the IPL sintered materials. The formation of CZTS film can be accomplished within a few minutes, which is nearly 60 times faster than the traditional thermal process. Furthermore, methylene blue photodegradation experiments were carried out to confirm the photocatalytic properties of IPL sintered CZTS films.

©Copyright by Cheng Zeng

November 30, 2018

All Rights Reserved

Formation of $\text{Cu}_2\text{ZnSnS}_4$ Thin Films via Reactive Sintering of Binary Metal-Sulfide
Nanoparticles Using Intense Pulsed Light

by
Cheng Zeng

A THESIS

submitted to

Oregon State University

in partial fulfillment of
the requirements for the
degree of

Master of Science

Presented November 30, 2018

Commencement June 2019

Master of Science thesis of Cheng Zeng presented on November 30, 2018

APPROVED:

Major Professor, representing Chemical Engineering

Head of the School of Chemical, Biological, and Environmental Engineering

Dean of the Graduate School

I understand that my thesis will become part of the permanent collection of Oregon State University libraries. My signature below authorizes release of my thesis to any reader upon request.

Cheng Zeng, Author

ACKNOWLEDGEMENTS

Firstly, I would like to express my sincerely appreciation to my advisor Dr. Chih-hung Chang for his enormous help and guidance. Also, I would like to thank Dr. Rajiv Malhotra for his help in intense pulse light sintering process. Without the help form these two professors I cannot finish my research.

Thanks to Michael Dexter for helping me to do the experiment on sintering. Thanks to Dr. Changqing Pan for discission on designing and testing in my whole research. Thanks to Dr. Yujuan He and Dr Zhongwei Gao for the help of scaanning electron microscope and transmission electron microscope.

Thanks for the support form National Science Foundation Civil, Mechanical and Manufacturing Innovation under award number 1537196.

Thanks to every group member in Chang's Group: Dr. Ki-joong Kim, yujing Zhang, Zhongwei Gao, Han Mei, Shujie Li, Ziyang Liu, Yu Cao, Jiayi Du, Hao Sun, and Tianlei Li. Last but not least, I would like to thank my parents, Tieming Zeng and Jianqing Li. Thanks for all the support of my parents done to me.

TABLE OF CONTENTS

| | <u>Page</u> |
|--|-------------|
| Chapter 1 Background | 1 |
| 1.1 Energy consumption and solar energy increasement | 1 |
| 1.2 Brief history of solar cell | 2 |
| 1.3 Material in solar cell | 3 |
| 1.4 CZTS | 4 |
| 1.5 Deposition methods | 5 |
| 1.5.1 Vacuum deposition approaches | 5 |
| 1.5.2 Non-vacuum deposition approaches | 6 |
| 1.6 Conclusion | 7 |
| Chapter 2 Experiment | 8 |
| 2.1 Preparation of Binary Nanoparticles Mixture | 8 |
| 2.1.1 Preparation of Binary Nanoparticles | 8 |
| 2.1.2 Preparation of unsintered samples | 10 |
| 2.2 sintering process | 16 |
| 2.2.1 Intense pulsed light(IPL) sintering | 16 |
| 2.2.2 UV Curing | 19 |
| 2.2.3 Xenon lamp sintering | 20 |
| 2.3 Methylene blue degradation | 21 |
| 2.3.1 Introduction | 21 |
| 2.3.2 Experimental process | 22 |
| Chapter 3 Characterizations | 24 |
| 3.1 Binary nanoparticles | 24 |
| 3.1.1 Raman result | 24 |

TABLE OF CONTENTS(continued)

| | <u>Page</u> |
|--|-------------|
| 3.1.2 Edax result | 25 |
| 3.2 IPL samples..... | 27 |
| 3.2.1 XRD result of IPL samples | 30 |
| 3.2.2 UV-VIS result of IPL samples | 31 |
| 3.2.3 Raman result of IPL samples | 32 |
| 3.2.4 SEM results of IPL samples..... | 33 |
| 3.2.5 TEM result of IPL samples | 36 |
| 3.2.6 Hall effect result of IPL samples..... | 36 |
| 3.2.7 Methylene blue degradation result..... | 37 |
| Chapter 4 Conclusion and future plan | 40 |
| Reference: | 41 |

LIST OF FIGURES

| <u>Figure</u> | <u>Page</u> |
|--|-------------|
| Figure 1.1 New U.S. Electricity Generating Capacity Additions, 2010-Q1 2018 | 2 |
| Figure 2.1 Microreactor system to produce binary nanoparticles..... | 9 |
| Figure 2.2 Tin(II) chloride in 30% HCl then dilute (Left) vs tin(II) chloride in water then add 30% HCl (Right) | 10 |
| Figure 2.4 Schematic diagram of printing process | 13 |
| Figure 2.5 Photos of fresh made inks (Left) and ink after 24 hours (Right)..... | 14 |
| Figure 2.6 SEM image of printed sample(Left) vs optical microscope image of spin coated sample(Right) | 14 |
| Figure 2.7 Boundary view of printed sample..... | 15 |
| Figure 2.8 Elemental distribution for printed sample | 15 |
| Figure 2.9 Schematic diagram of an IPL system | 17 |
| Figure 2.10 Photo of IPL samples..... | 18 |
| Figure 2.11 Outside(Left) and inside(Right) view of UV curing system setup | 19 |
| Figure 2.12 Schematic diagram of xenon lamp sintering | 20 |
| Figure 2.13 Schematic diagram of methylene blue degradation under light via photocatalyst | 21 |
| Figure 2.14 Schematic diagram for methylene blue degradation experiment | 23 |
| Figure 3.1 Raman results of a) CuS, b) ZnS, c) SnS nanoparticles | 25 |
| Figure 3.2 EDAX results of a) CuS, b) ZnS, c) SnS..... | 27 |
| Figure 3.4 XRD results of IPL samples | 30 |
| Figure 3.5 UV-Vis result for IPL samples..... | 31 |
| Figure 3.6 Tauc's plot of IPL samples | 32 |
| Figure 3.7 Raman result of IPL samples..... | 33 |

LIST OF TABLES

| <u>Table</u> | <u>Page</u> |
|---|-------------|
| Table 1.1 Element abundance of ordinary solar materials | 4 |
| Table 2.1 Experiment conditions for IPL samples | 18 |
| Table 3.1 Experimental condition of IPL samples | 29 |
| Table 3.2 Hall effect result of IPL samples | 37 |

Roll to Roll Process Design for Cu_2ZnSnS_4 Thin Film via Intense Pulsed Light Sintering

Chapter 1 Background

1.1 Energy consumption and solar energy increasement

The global economy is growing faster and faster these days. In 2017, the world economy grew at 3.1% which achieved the fastest growth rate since 2011. However, the world economy is built upon the energy market. In 2017, primary energy consumption growth averaged 2.2% which achieved the fastest growth rate since 2013. Since the fossil fuels in the world are limited, more and more people focus on the sustainable energy source. In 2017, renewable power grew by 17% (69 mtoe), higher than the last 10-year average. Renewable energy is playing a more and more important role in the energy market.¹⁻²

Among all sustainable energy, solar energy is always an important part. In fact, solar energy is the original source of most types of energy. Other two main sustainable energy, wind power and hydropower are derived from solar energy. Besides, solar energy does not need huge investment for the instruments.

In Q1 2018, the U.S. installed 2.5 gigawatts of solar photovoltaic (PV) capacity to reach 55.9 gigawatts of total installed capacity, enough to power 10.7 million American homes. This is a 13% increase which compares to last year. From Figure 1.1, it is clear that the size of solar energy power plant has a great increase from 2010 to 2018. The capacity of Q1 2018 almost is 40 times than the capacity in 2010. If this tendency continuous, total installed U.S. PV capacity is expected to more than double over the next five years, which

means 80 times the capacity in 2010. In 2023, over 14 gigawatts of PV capacity will be installed annually in the U.S.³

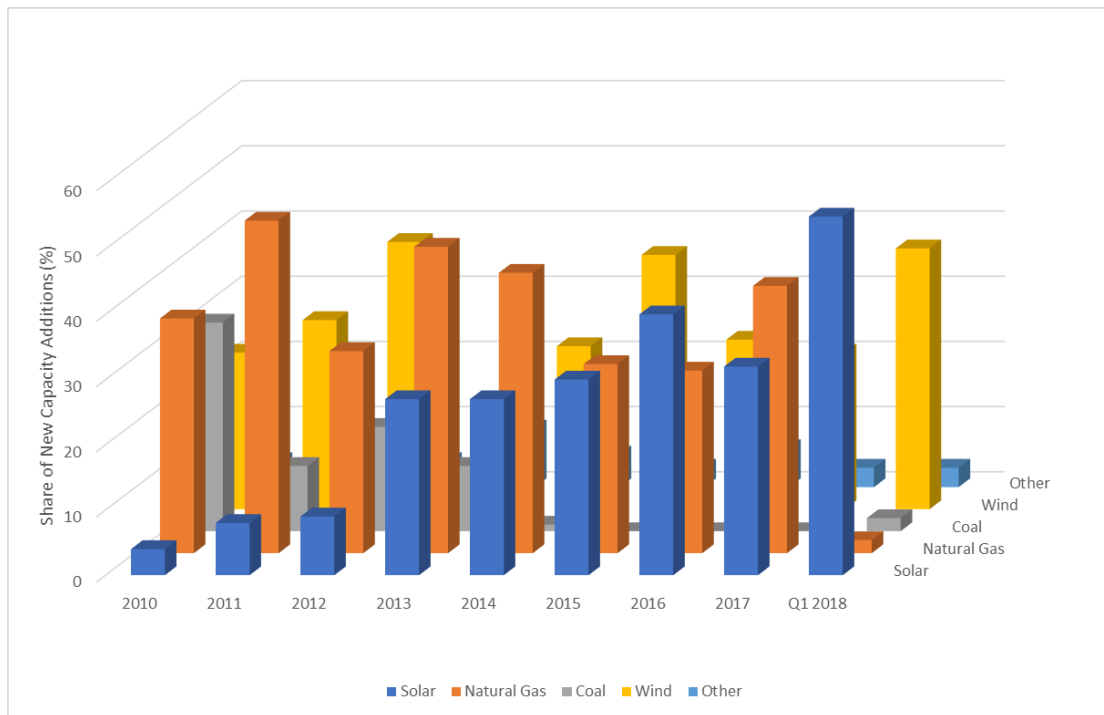


Figure 1.1 New U.S. Electricity Generating Capacity Additions, 2010-Q1 2018¹

1.2 Brief history of solar cell

The first solar cell was constructed in the 1880s by Charles Fritts which based on a method directly converts light to electric current using the photovoltaic effect. Then in the 1930s and 1940s, the scientists in German used chalcogenide to fabricate the solar cell which had very low conversion efficiency. In 1954, Calvin Fuller and Daryl Chapin created silicon solar cell which leads the main path of the solar cell commercialization. However, first solar cells cost a lot. These early solar cells cost 286 USD/watt and reached efficiencies of 4.5–6%.

Solar energy was firstly used in small and medium-sized applications like calculators and off-grid remote homes powered by a PV system. In the 1980s, people started to utilize solar power in large scale like a solar farm, which uses many solar panels to harvest light and

transform the solar energy to electricity. The largest solar power plant is the 1547 MW Tengger Desert Solar Park, in Ningxia, China by 2018.

1.3 Solar materials for solar cell

Nowadays, silicon is the most widely used material in the solar cells. The efficiency of single crystalline silicon (sc-Si) cell can reach 26.7% and the multi-crystalline silicon (mc-Si) cell can reach 22.3%.⁴ Also, silicon is an earth-abundant element which has very low cost. As a result, silicon will continue to dominate the large-scale use of the solar cell. However, silicon is presented in SiO₂ in the natural, and 1500°C is required for silicon smelting. Moreover, silicon is an indirect band gap material which need more than 300 micrometers thickness to maximally utilize the sunlight.⁵

Alternatively, direct band gap materials are used for thin film solar cells. Compare to silicon solar cells, they just need 1~2 micrometers thickness film to absorb the sunlight. Among all the materials, multi-elemental compounds are the most efficient materials which include GaAs (28.8%), InP (24.2%), CdTe (21.0%) and copper indium gallium selenide (CIGS) (21.7%). III–V group based material are the most efficient (almost 29%) but very expensive and hard to make because they are very hard to crystal in single crystalline style.⁶⁻⁷ CIGS and CdTe are relatively less efficient and far more cheaper than III–V group based material. Also, they are easier to fabricate than III–V based material. However, the core elements of these cells are Ga, In, and Te, which are expensive and low abundance in the earth's crust (table 1.1).⁸ Besides, Cd and Te are toxic and not environment-friendly.

As a replacement, Zn and Sn are used to replace In and Ga, which yields an earth-abundant, non-toxic material that can be used in thin film solar cells. CZTS or CZTSSe have been noticed in the research area. The CZTS films started from a very low efficiency and fast increased to 12.6%. Some scientist believed that this is a new solution of the energy problem which we are facing now.

Table1.1 Element abundance of ordinary solar materials³

| element | Cd | Cu | Ga | In | S | Se | Sn | Te | Zn |
|---|--------|--------|-----|------|--------|-------|---------|-------|--------|
| Abundance in the upper Continental crust(ppm) | 0.15 | 60 | 19 | 0.25 | 350 | 0.05 | 2.3 | 0.001 | 70 |
| 2016 worldwide production(tons) | 23,000 | 19,400 | 375 | 655 | 69,300 | 2,200 | 280,000 | 400 | 11,900 |

1.4 CZTS

The early synthesis of CZTS was reported by Ito in 1988 via the sputtering method. After that, CZTS appears in more and more papers. The efficiency of CZTS cells grows very fast: 10.1% in 2012, 11.1% also in 2012 and finally 12.6% in 2014.⁹ Highest efficiency of CZTS that has been reported in 2014 at IBM, Wang *et. al.* made a 12.6% efficiency CZTS solar cell through solution technique which used hydrazine as the solvent and soda-lime glass as substrate.¹⁰

Many methods can be used for CZTS thin film deposition, including e-beam and thermal evaporation, sputtering, pulsed laser deposition (PLD), spray pyrolysis, photochemical deposition (PCD), electrochemical deposition (ECD), sol-gel methods, solution methods and chemical vapor deposition (CVD).¹¹

Besides the advantages in the field of solar cell, CZTS can also be used in water splitting and photonic catalyst with favorably matched band gap (1.1–1.6 eV) to solar spectrum, high absorption coefficient in the visible range ($\geq 10^4 \text{ cm}^{-1}$), low toxicity, good photostability, and relative abundance of the component elements.^{9,11}

1.5 Deposition methods

The deposition methods can be classified into two main categories: vacuum deposition methods and non-vacuum deposition methods. Basically, vacuum deposition methods can create more uniform film with better morphology. However, the cost of vacuum deposition methods is much higher than non-vacuum methods. Here is a brief discussion of all the coating methods.

1.5.1 Vacuum deposition approaches

1.5.1.1 E-beam evaporation

This method uses an electron gun which emits electrons to strike the evaporation material generating vapor which will deposit on the substrate. It provides precise control at the ratio of the material but is expensive because it needs high accelerating voltages. Many groups have used this method to synthesize CZTS. The highest efficiency that used this method was in 2016, from Shin's group which achieved 8.4%.¹²

1.5.1.2 Sputtering

Sputtering is a process whereby particles are ejected from a solid target material due to bombardment of the target by energetic particles, particularly gas ions in a plasma. Additionally, some other elements besides the main precursors have been used to improve the quality of the film but did not provide much improvement.¹³⁻¹⁵

1.5.1.3 Pulsed laser deposition (PLD)

PLD is an alternative process in which a KrF laser beam is used to ablate pellets of CZTS and whose fragments are deposited on the substrates at 300 and 400°C. The deposition of

CZTS films are confirmed by p-XRD. Pawar's group has researched the relationship between laser energy and optical properties of CZTS thin films.⁹

1.5.2 non-vacuum deposition approaches

1.5.2.1 spray pyrolysis

Spray pyrolysis is a method that sprays the precursors at the heated substrate. During the spray the solution will evaporate. This is a potential suitable method for large area application because it has very low cost. However, this method requires the precursor can be dissolved into solution and the solution is also restricted because it need to be totally evaporated before the whole reaction.¹⁶⁻¹⁸

1.5.2.2 Photochemical deposition (PCD)

PCD is a method that uses precursors aqueous solution and illuminates with high power light source, usually UV light. Moriya's group used CuSO_4 , ZnSO_4 , SnSO_4 and NaS_2O_3 as precursor and illuminated by deep-UV light for 1h and obtained CZTS thin film with low intensity XRD peaks.¹⁹⁻²⁰

1.5.2.3 Electrochemical deposition (ECD)

ECD is another potential method that can be used for CZTS thin film deposition. Films were made from metallic layers, Cu, Zn and Sn electrochemically deposited using a conventional 3-electrode cell with a platinum counter electrode. Then annealed in a sulfur atmosphere to form a CZTS film. Total process is cheap but needs sulfur atmosphere which may be danger to the environment.²¹⁻²³

1.5.2.4 Solution methods

Solution methods are also very cheap. They use metal salts as precursors which can be dissolved in solution. Then the solution is directly reacted with elemental sulfur to form dispersible nanoparticles. The solution is coated to any substrate and heated to form CZTS films. The size and morphology of the film is districted by the heating method. Also, the particles are hard to form film, so this method often makes very thick and low efficient films.²⁴⁻²⁶

1.6 Conclusion

The method used in this thesis is a combination of solution method and photochemical method. To make a roll to roll process, two main steps are needed. The first step is making nanoparticles from the precursors and make thin films with these nanoparticles. Then using photonic sintering to form CZTS films which can be used in solar cell or other applications. Previously, the goal of this experiment is to make a solar cell. However, as the limitation of the time, the experiment on photocatalysis of the thin film has been done instead of making solar cell.

Chapter 2 Experiment

We proposed a very quick and efficient process for producing CZTS thin film which consists of three main steps: preparation of binary nanoparticles mixture ink, deposition of thin film, followed by the sintering process. Ideally 200 m²/hr manufacturing rate can be achieved by this process.

2.1 Preparation of Binary Nanoparticles Mixture

2.1.1 Preparation of Binary Nanoparticles

The first step of the whole process is the preparation of binary nanoparticles. The binary particles are prepared by a high output continuous microreactor system (Figure 2.1). Briefly, metal precursor and the sulfur source are dissolved in the water and continuously pumped into the micromixer. A gas-liquid segment system is used by introducing gas into the micromixer to prevent the clogging of the whole system. By controlling the length of the microchannel and the flow rate, the particle size can be controlled between 80 nm and 200 nm which fits the need of the next step.²⁷ Each kind of binary nanoparticles is obtained at a rate over 320 g/hr which can yield a production rate of CZTS at 1000g/hr. For a common CZTS thin film solar cell, 1 m² solar cell needs about 5 g CZTS nanoparticles, so this system can produce 200 m² CZTS thin film for solar cell in one hour.

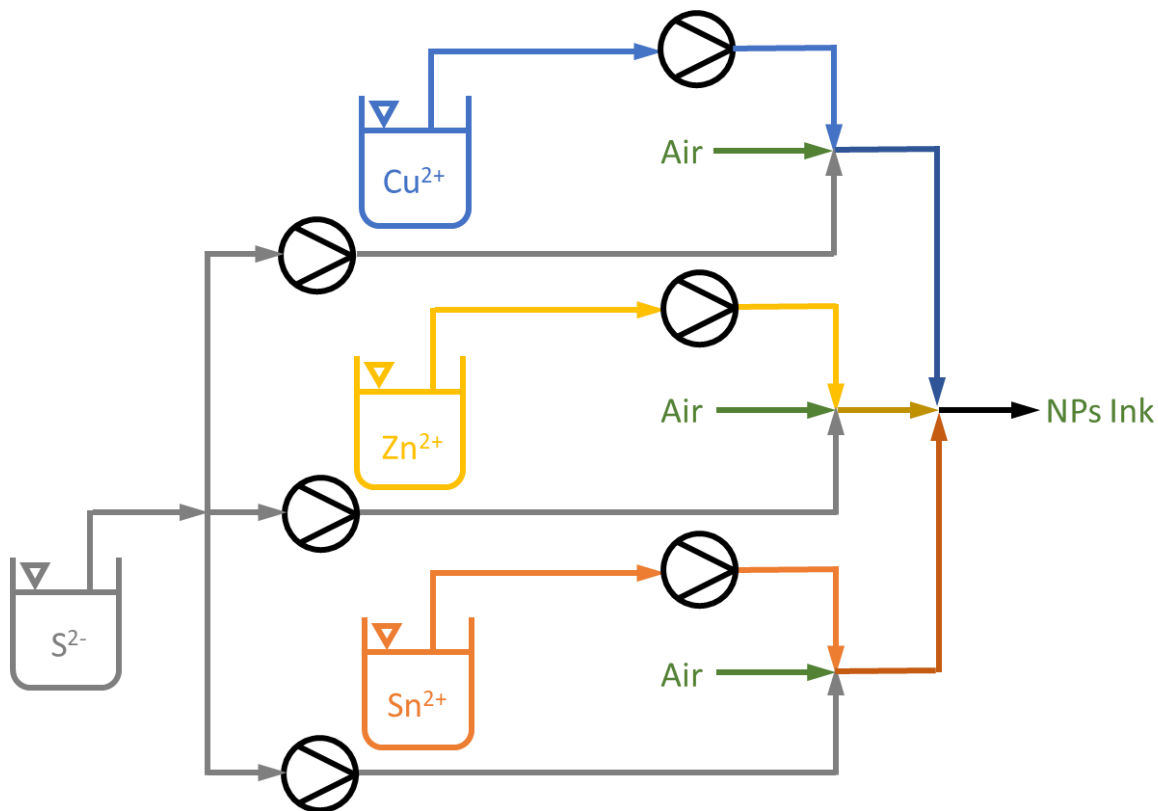


Figure 2.1 Microreactor system to produce binary nanoparticles

The syntheses of copper sulfide (CuS) and zinc sulfide (ZnS) are similar. Copper(II) acetate and zinc acetate have been used as metal precursors and introduced to the micro-mixer in the microreactor system. After this very quick mixing, CuS and ZnS nanoparticles are washed by DI water and ethanol, each three times, then centrifuged and vacuum-dried to powder. Meanwhile, tin(II) chloride is easily hydrolyzable (Figure 2.2), so tin(II) chloride is firstly dissolved in 30 wt.% HCl solution then diluted with DI water. Also, more sodium sulfide is added in to react with HCl in the tin sulfide synthesis. The wash and the separate process for tin(II) sulfide (SnS) is the same as other two metal sulfides.

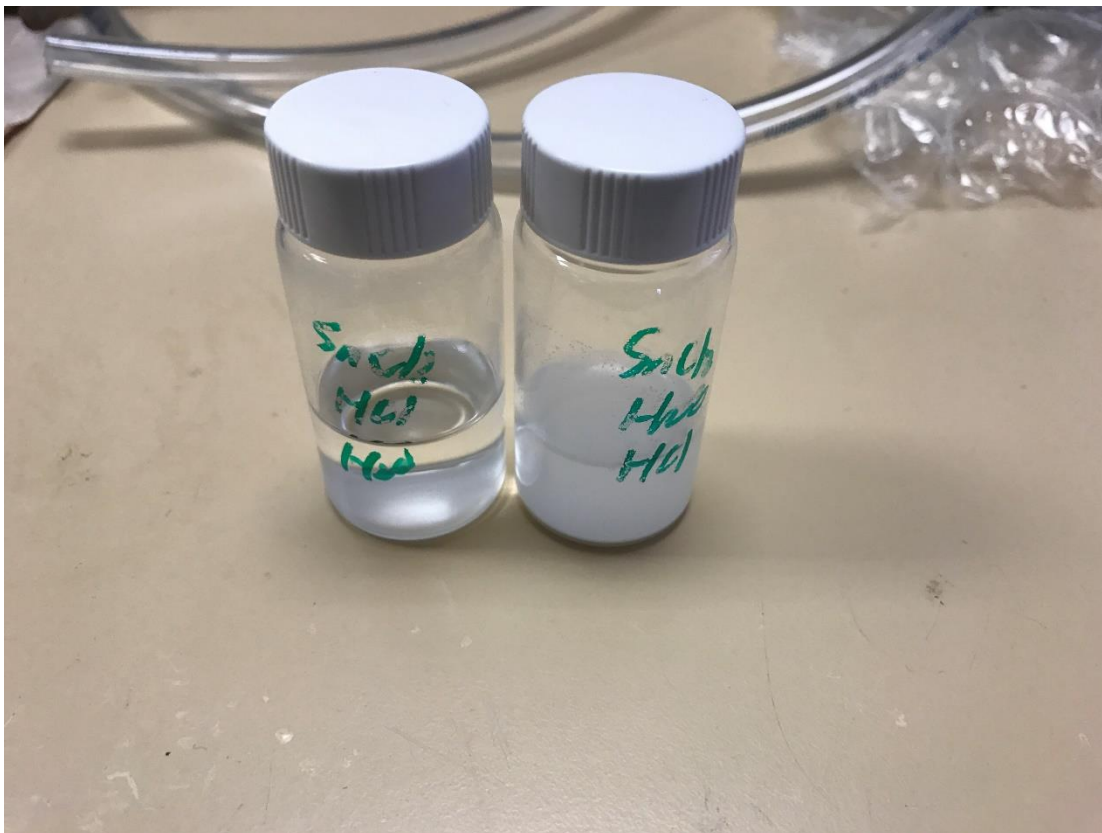


Figure 2.2 Tin(II) chloride in 30% HCl then dilute (Left) vs tin(II) chloride in water then add 30% HCl (Right)

2.1.2 Preparation of unsintered samples

The next step is using the nanoparticles from pervious step to make thin films. To improve the quality and reduce the cost, many methods have been tried but two different methods which all belong to non-vacuum methods were finally chosen.

2.1.2.1 Trial of coating methods

A lot of methods have been used to make the thin film from nanoparticles. Firstly, three binary nanoparticles and additional thiourea were dispersed in a solution combined by 80 vol.% 2-Methoxyethanol (2-ME) and 20 vol.% Monoethanolamine (MEA). Then 1%~20%

polyvinylpyrrolidone (PVP) is added to adjust the viscosity of the solution to form the precursor that can be used. After several unsuccessful trails of drop casting and doctor blade coating, we found that the viscosity of the precursor is too high for the drop casting and too low for the doctor blade. The samples made from drop casting are usually just particles while the samples from doctor blade are too thick (several millimeters) so other methods have been chosen for making a thin film.

2.1.2.2 Spin coating

The first successful method to make the thin film is the spin coating method. It is a method that applies a small amount of coating material to a spinning substrate. To adjust the viscosity of the coating material and the thickness of the thin film (Figure 2.3), the concentration of the precursor, the amount of the PVP, the coating layers and the coating conditions have been tested and confirmed. It was found that 2-ME is a good solution and the MEA is a good stabilized material in the system. Therefore, the solution of the precursor is combined by 80 vol.% 2-ME and 20 vol.% MEA. According to Guo *et. al.*, to form a CZTS film the precursor should have a copper-poor and zinc-rich stoichiometry.²⁸⁻²⁹ Compared to the original stoichiometry of copper, zinc, tin and sulfur in the CZTS is 2:1:1:4, in this process, the mass of CuS, ZnS, and SnS are 0.57 g, 0.35 g, and 0.47 g, respectively, which yields an elemental ratio of Cu:Zn:Sn at 1.91:1.15:1, similar to the result reported by Kim *et. al.*²⁷ Then additional 0.24 g thiourea is added as an extra sulfur source and 0.05 g PVP is added to control the viscosity of the precursor. After 2-hour sonication, this precursor is coated to glass and/or silicon substrate under these conditions: the amount of precursor: 5 μ l, the speed of spinning: 2500 rpm, the coating time: 30 seconds, the coating layers: 2 layers, the waiting time between layers: 45 seconds, the time for drying in the vacuum oven: 2 hours.

After vacuum drying, the thickness of the product is 1~1.5 μm and the elemental ratio of copper, zinc, tin, and sulfur is suitable. Figure 2.3 shows the top view of the thin film through the microscope. It shows that the morphology of the thin film is not so good because of two reasons. Firstly, the coffee ring effect is obvious in Figure 2.3a, so the material will be very thick in the middle and the edge. Secondly, the whole film is not uniform, the thickness is varying on the micrometers scale. CuS, ZnS, and SnS cannot be dissolved in the solution but thiourea can be dissolved so when the thiourea crystallized the uniformity of the film will be broken. After all, the morphology of the thin film will be not so good.

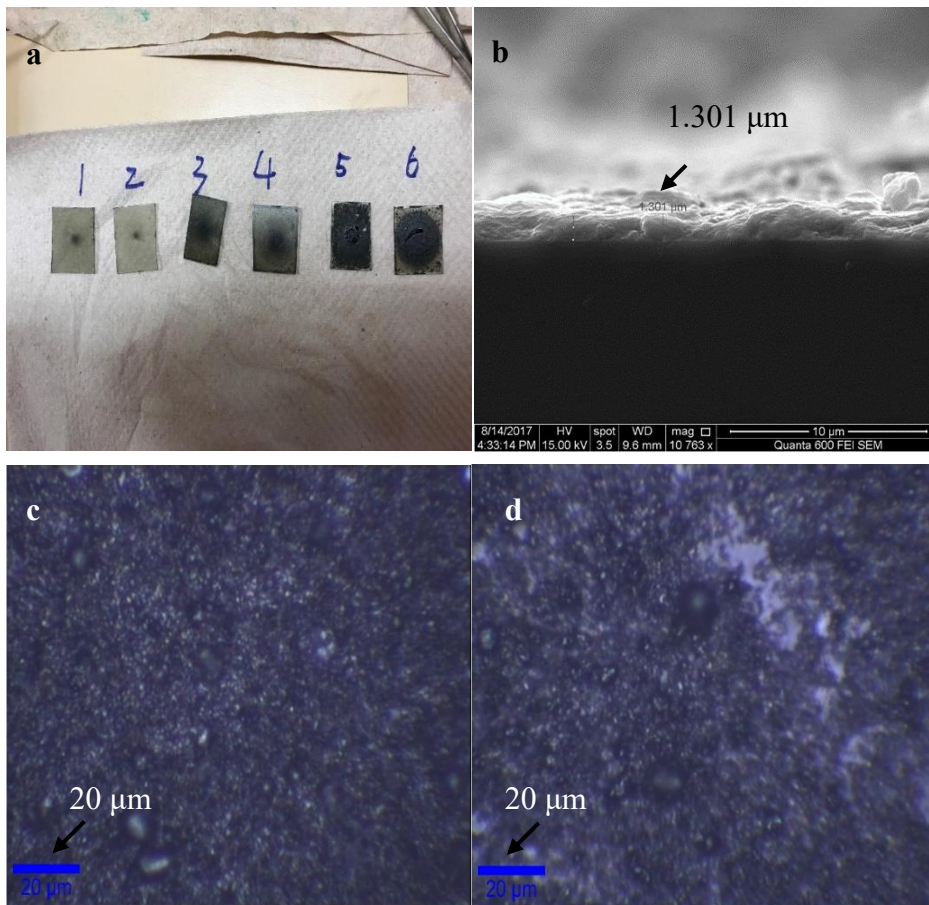


Figure 2.3 a) Photos of unsintered samples; b) SEM image of unsintered samples; c) & d) Optical microscopy view of unsintered samples

2.1.2.3 Inkjet printing

According to the optical and SEM images, we conclude that the morphology of the thin film made by spin coating is not so good. Therefore, inkjet printing have been used to improve the morphologic quality of the thin film. Figure 2.4 Shows a sketch map of the inkjet printing process.

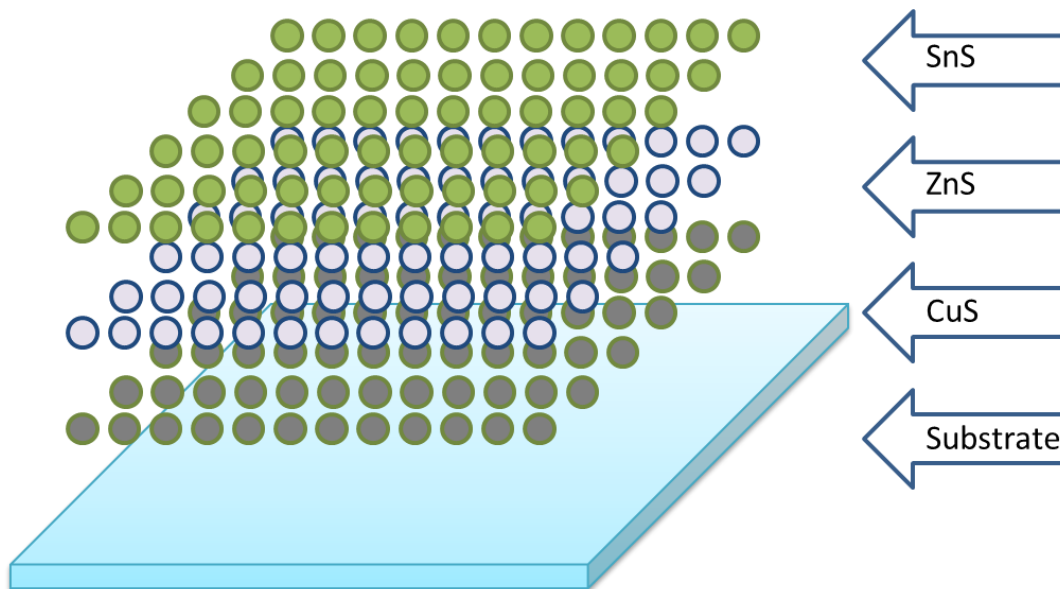


Figure 2.4 Schematic diagram of the printing process

The basic method of inkjet printing is to print the three kinds of binary nanoparticles layer by layer to form a thin film by digital material inkjet printer. Since the printing process is more controllable than spin coating, the morphology of the thin film is better. Although the coffee ring effect cannot be eliminated by controlling the size and concentration of every single droplet and the printing speed, the coffee ring effect by each individual droplet can be covered by following droplets, so the overall morphology of the whole film is better. Different binary nanoparticles are printed separately, additional thiourea is added after printing of all binary nanoparticles. All the binary nanoparticles are dispersed in the 80 vol.% 2-ME and 20 vol.% MEA solution and sonicated before being loaded to the cartridges. All the inks are unstable under the ambient protective condition, so the whole process needs to

be done in a short time frame. Figure 2.5 shows the comparison of the fresh prepared ink and the inks after 12 hours. The size of the droplet, printing speed, charging model of the inkjet printer, concentration of the precursors and temperature of the substrate were studied to yield a suitable way for printing.



Figure 2.5 Photos of fresh made inks (Left) and ink after 24 hours (Right)

Figure 2.6 (Left) shows the scanning electron microscope(SEM) result of the printed sample. It is obvious that the morphology is much better than the spin-coated samples. The printed samples are more uniform on the micrometers scale.

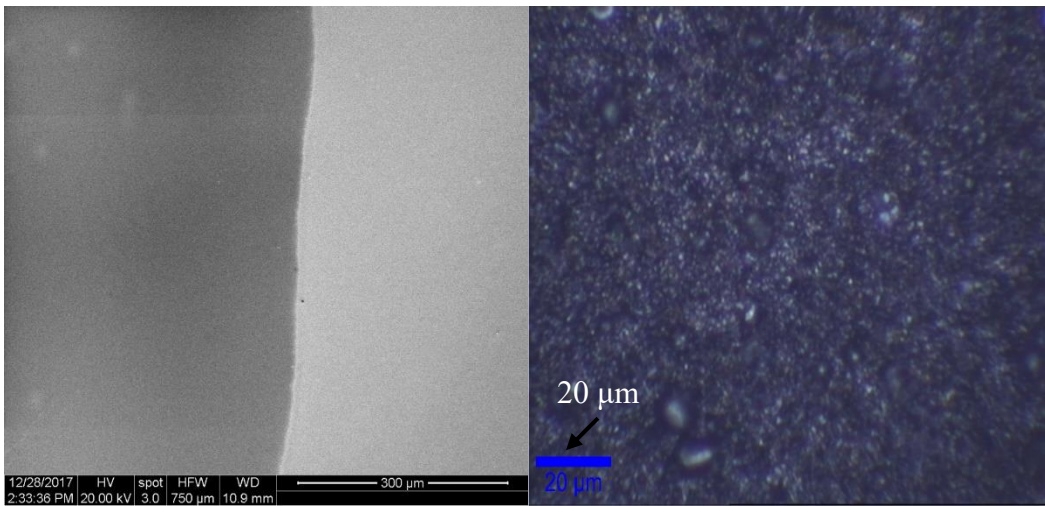


Figure 2.6 SEM image of printed sample(Left) vs optical microscope image of spin coated sample(Right)

Also, EDX (energy-dispersive X-ray spectroscopy) measurement has been used to check the elemental distribution of the thin film. Figure 2.8 shows the EDX elemental mapping

of a printed thin film. As shown in the pictures, all copper, zinc, tin, and sulfur are dispersed almost the same. However, as the film still have some impurity and the sulfide mapping is different, the printing process need more development.

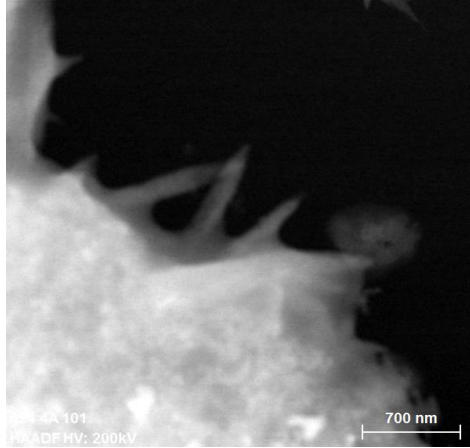


Figure 2.7 Boundary view of printed sample

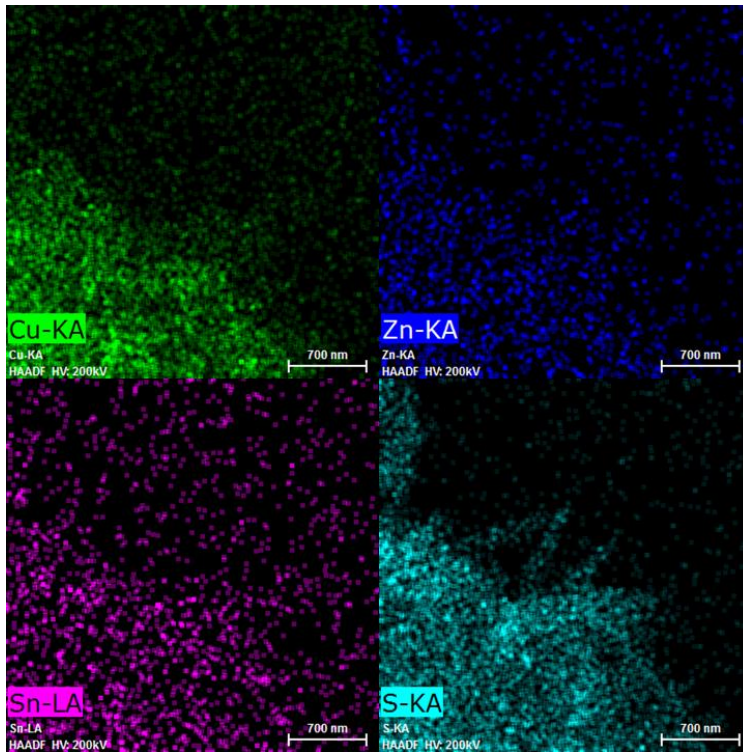


Figure 2.8 Elemental distribution for printed sample

2.2 Sintering process

The target of the sintering process is to convert the binary nanoparticles film to CZTS quaternary thin film. To improve the time and minimize the cost different photonic methods have been studied.

2.2.1 Intense pulsed light (IPL) sintering

2.2.1.1 Brief introduction of the instrument

A brief diagram of the IPL system is shown in Figure 2.9. Basically, this whole system consists of a powerful xenon lamp (400~700nm) and a driving part. The xenon lamp has an working output up to dozens of joules per one square centimeter. When the sample is very big the driving part can transport the whole sample at a certain speed to make every part of the sample evenly sintered. This experiment uses a pulse model which means its outputs of the energy in a very short time is very high.

When compared to other methods that make CZTS on a time budget, the IPL method is very fast. The conventional thermal annealing process costs more than one hour and some of them cost four or more hours when including the ramping up and cooling down stages. The microwave method often needs more than 30 mins.³⁰⁻³³ While one pulse of IPL just needs several seconds, and this method needs no more than 20 pulses, which means one process need no more than 1 minute, just 1/30~1/240 of the regular methods. Also, the energy input to the system is very high in very short time. Thus, the system can be heated to a very high temperature which can make the reaction happen.

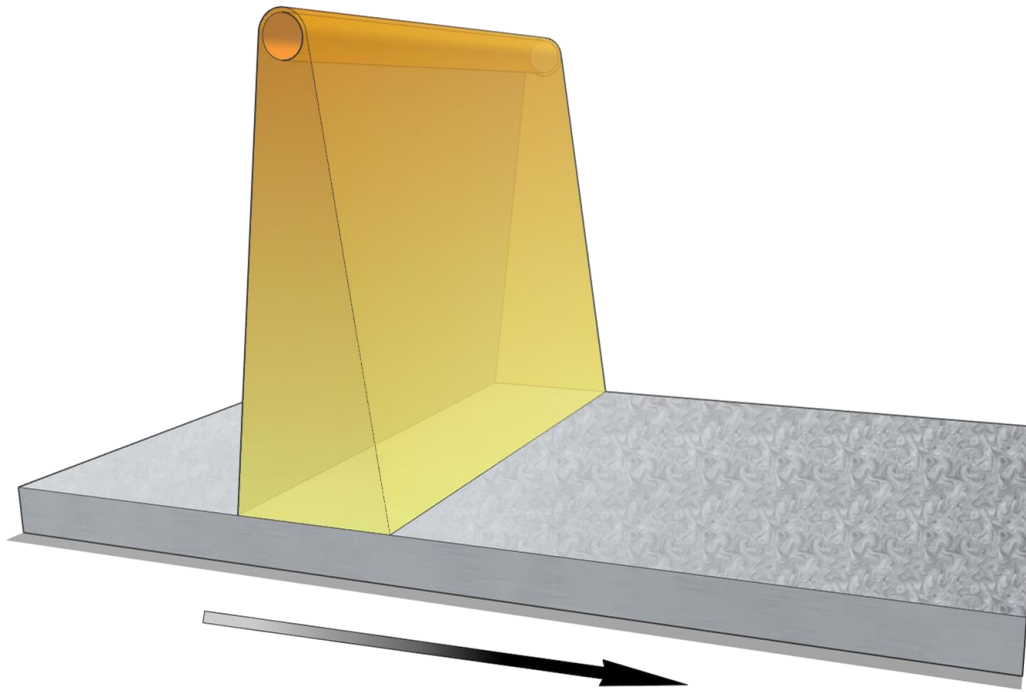


Figure 2.9 Schematic diagram of an IPL system

2.2.1.2 Experimental conditions

By changing the sintering power and pulses the samples have been sintered. The conditions of the experiment are shown in Table 2.1.

The temperature here is very important during the process. Higher the temperature, faster the reaction. When the temperature is lower than 250°C , the CZTS cannot be formed at all. When the temperature over 450°C CuSnS_3 will be the main product so all the process here is controlled less than 450°C .³⁴⁻³⁵

The photos of the after sintering samples are shown in Figure 2.10. All these samples are from the spin coating method so the coffee ring effect is obvious in all the samples. After sintering all the samples turned from brown to dark brown or black. Also, when the temperature and the input energy is increased, the whole sample will be darker and more burned.

Table 2.1 Experiment conditions for IPL samples

| Sample number | sintering energy (J/pulse) | sintering pulses | Average temperature (°C) |
|---------------|-------------------------------|------------------|-----------------------------|
| 1 | 10 | 5 | 258.3 |
| 2 | 10 | 10 | 281.8 |
| 3 | 10 | 20 | 351.1 |
| 4 | 16 | 5 | 367.6 |
| 5 | 16 | 10 | 357.5 |
| 6 | 16 | 20 | 417.1 |
| 7 | 20 | 5 | 409.3 |
| 8 | 20 | 10 | 435.6 |
| 9 | 20 | 20 | 444.4 |

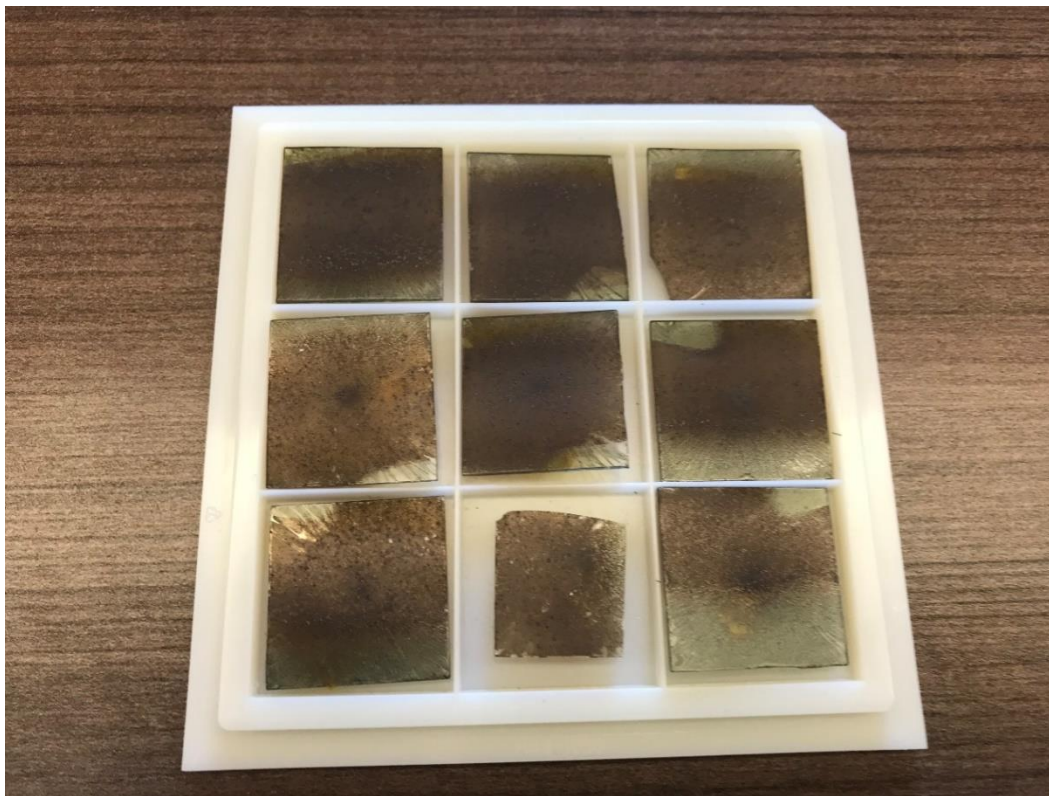


Figure 2.10 Photo of IPL samples

2.2.2 UV curing

2.2.2.1 Brief introduction of instrument

To identify if the precursor can be sintered under the higher energy light source or not, UV source has been introduced into the experiment. The light source of UV curing is Omnicure series 2000. The irradiance level is $0.2\sim 40\text{ W/cm}^2$ and the wavelength is $320\sim 500\text{ nm}$. The whole system is shown in Figure 2.11a. The left part is the light source and the UV light is transmitted through the optical fiber to the dark box. Figure 2.11b shows the inside part of the dark box. The UV light is directly shining over the sample which is held on a high-quality isothermal foam. The distance from the fiber endpoint to the sample is 3 cm to ensure the light spot can cover the whole sample. Also, a test sample is putted into the system to confirm the location of UV light to ensure the place of the sample.



Figure 2.11 Outside (Left) and inside (Right) view of UV curing system setup

2.2.2.2 Experimental conditions

For this experiment, spin-coated samples have been used as precursors. From 2 mins to 60 mins, a series of experiments have been done every 5 mins. However, according to XRD

results, there is just very low CZTS peaks in 10 mins samples and no CZTS peaks for other samples. As a result, this light source was determined not suitable for converting binary nanoparticles mixture into CZTS thin film.

2.2.3 Xenon lamp sintering

2.2.3.1 Brief introduction of instrument

To confirm if the sample can be sintered under the original light source or not a process of ordinary xenon lamp test were done. A schematic diagram that shows the setup of the xenon lamp sintering is shown in Figure 2.12. The idea here is using a xenon lamp as a light source that tries to sinter the precursor without the high energy input.

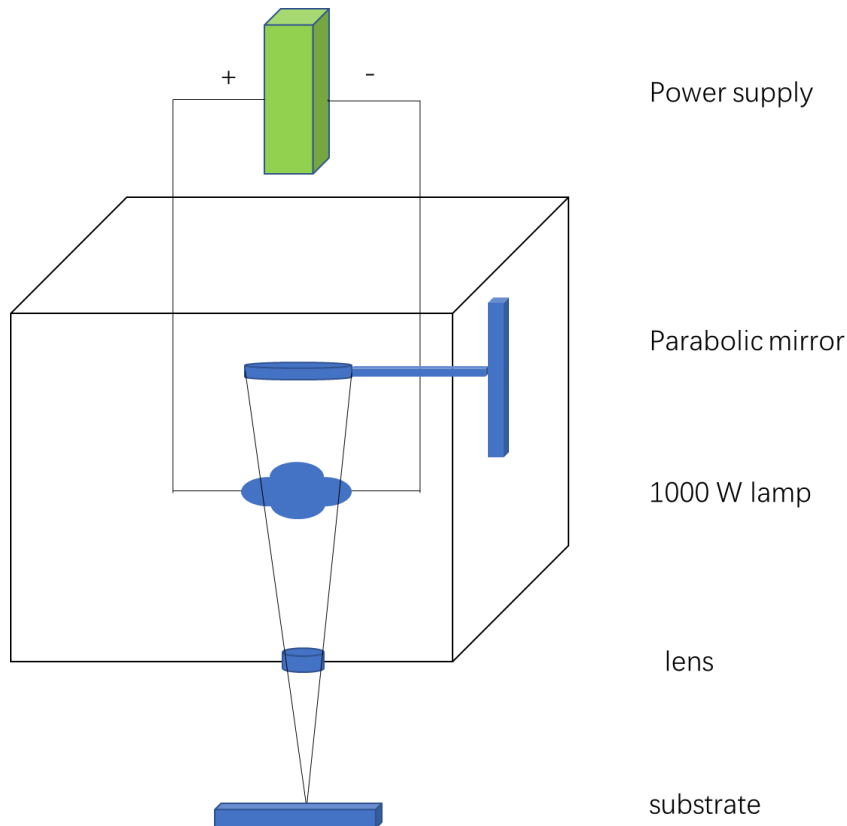


Figure 2.12 Schematic diagram of xenon lamp sintering

2.2.3.2 Experimental process

In this experiment, spin-coated samples have been used as precursors. From 5 mins to 30 mins, a series of experiments have been done every 5 mins. However, according to XRD results, there are no CZTS peaks for any of the samples. As a result, this light source is not suitable for CZTS synthesis.

In total, the only suitable light source of this experiment is IPL light source.

2.3 Methylene blue degradation

2.3.1 Introduction

CZTS is a good photocatalyst as a p-type material.^{10, 36-37} However, as the time limit, this process just uses the degradation of methylene blue as an example. A brief graph that shows the reaction of degradation is in Figure 2.13

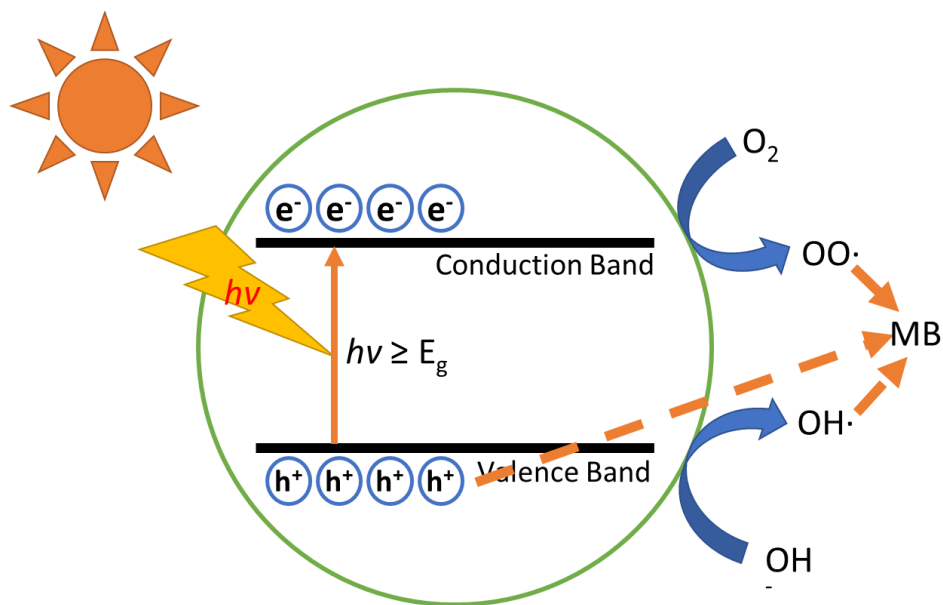
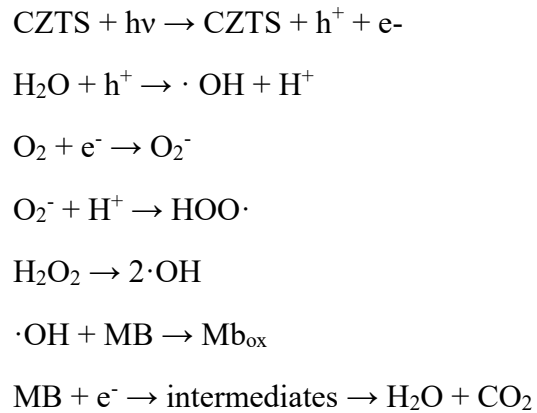


Figure 2.13 Schematic diagram of methylene blue degradation under light via photocatalyst

As a p-type photonic catalyst, when absorbing visible or UV light, the CZTS nanoparticle film will generate holes and electrons. Then the water and the water-dissolved oxygen can react with the holes and electrons to generate radicals. Then the radicals will react with methylene blue which will cause the degradation of the methylene blue. The possible mechanism of the methylene blue's degradation is shown below.³⁸



2.3.2 Experimental process

The schematic diagram of the experiment setup is shown in Figure 2.14. The liquid here is the 1×10^{-6} mol/L methylene blue aqueous solution. The light source here is xenon solar simulator which represents the sunshine.

For each sample, a 4 hours experiment has been done to test the photocatalytic degradation. The solution was sampled every hour to measure the concentration of the methylene blue by UV-Vis.

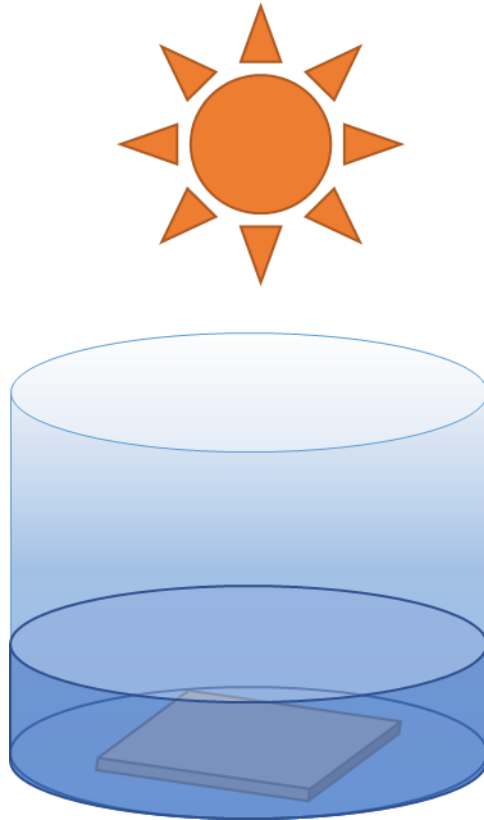


Figure 2.14 Schematic diagram for methylene blue degradation experiment

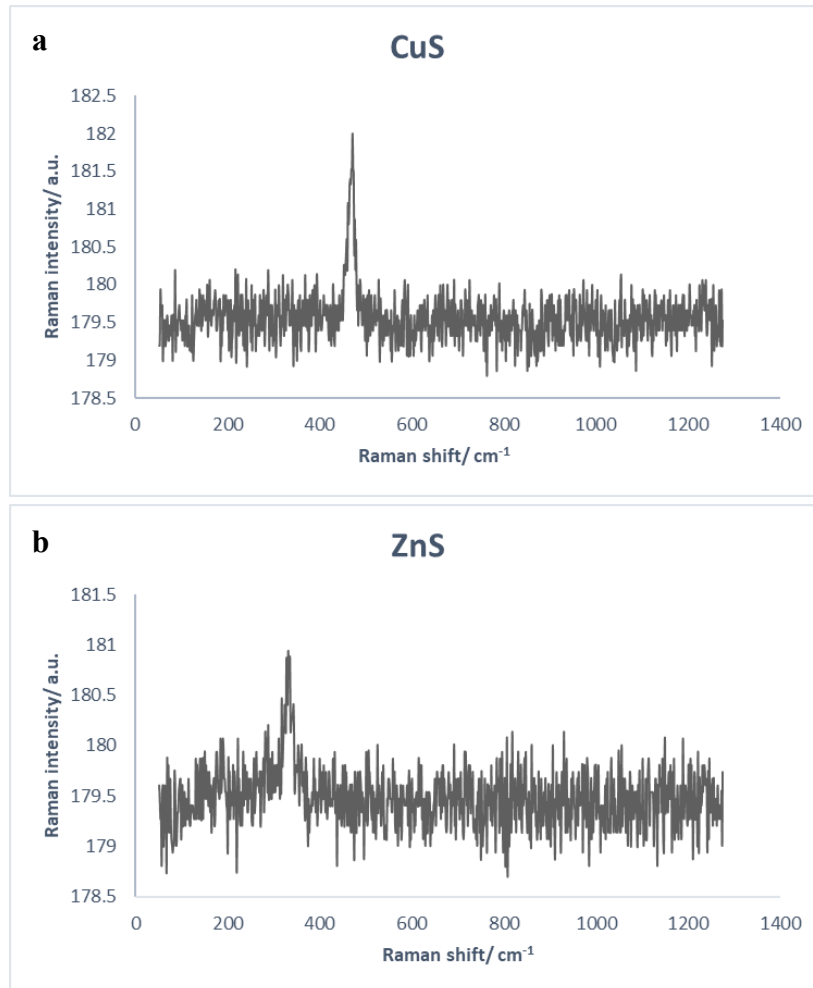
Chapter 3 Characterizations

3.1. Binary nanoparticles

3.1.1 Raman results

Raman (WITEC Alpha 300a confocal Raman microscope) and EDAX have been used to identify the quality of the binary nanoparticles.

The images in Figure 3.1 show the Raman test result of these three kinds of binary nanoparticles.



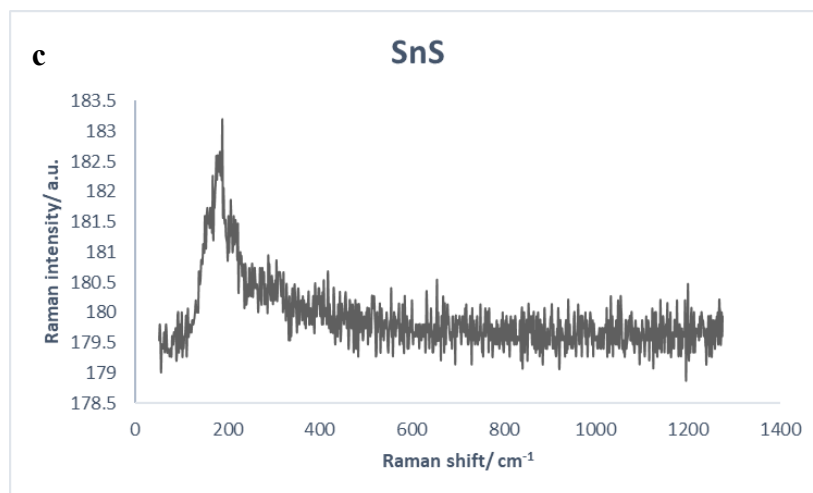


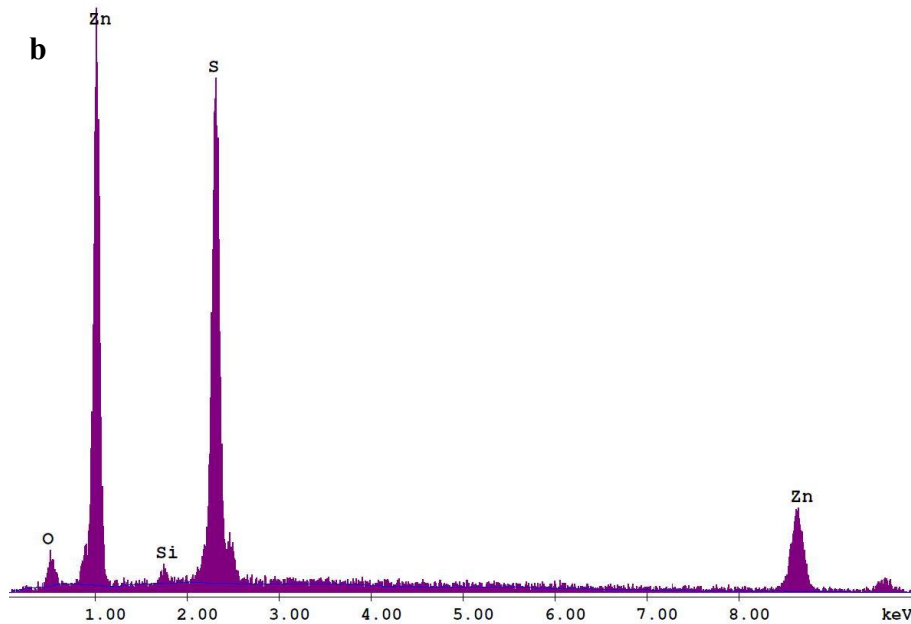
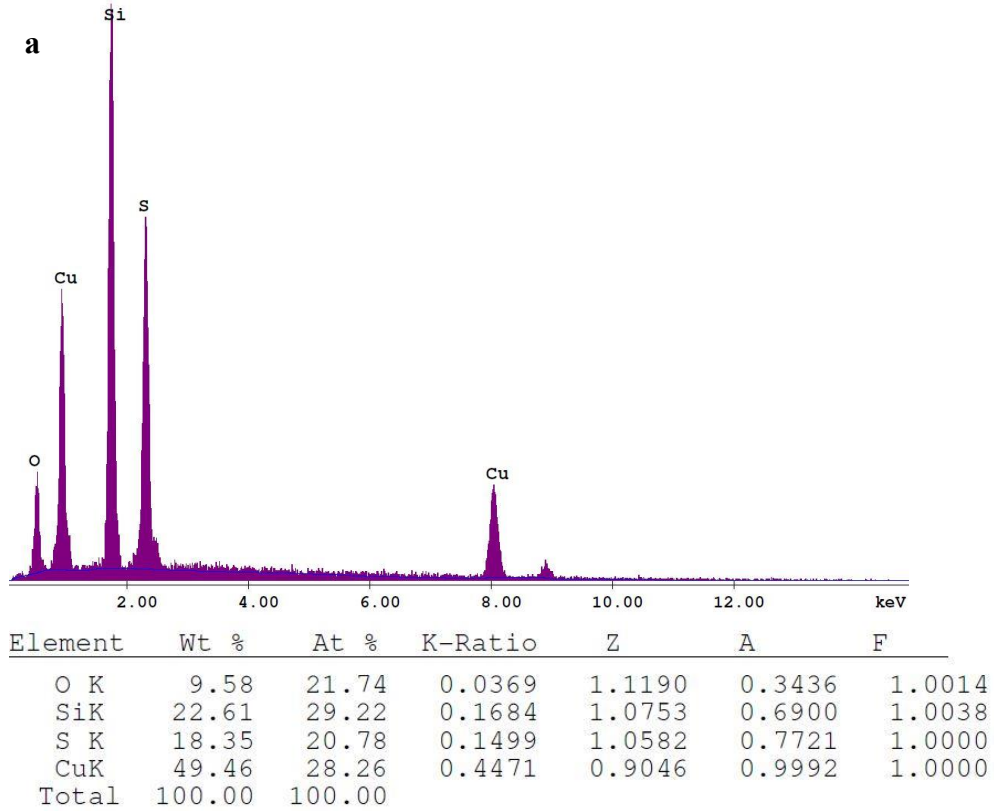
Figure 3.1 Raman results of a) CuS, b) ZnS, c) SnS nanoparticles

The Raman results of these three binary nanoparticles have been shown in Figure 3.1. These nanoparticles are drop cast on the substrate so the crystal size should not be very big but at nano scale. As a result, although the Raman can detect these nanoparticles the signal is not very strong. The S-S peak in the CuS is at 470 cm^{-1} , as shown in Figure 3.1(a). These Raman peaks are matches the reference.³⁹ The S-S stretch band was the dominant feature of the spectrum from the surface when the potential was increased into the region in which covellite CuS is formed. Also, the peak at 340 cm^{-1} in Figure 3.1(b) and the peak at 180 cm^{-1} in Figure 3.1(c) prove the nanoparticles are ZnS and SnS respectively.

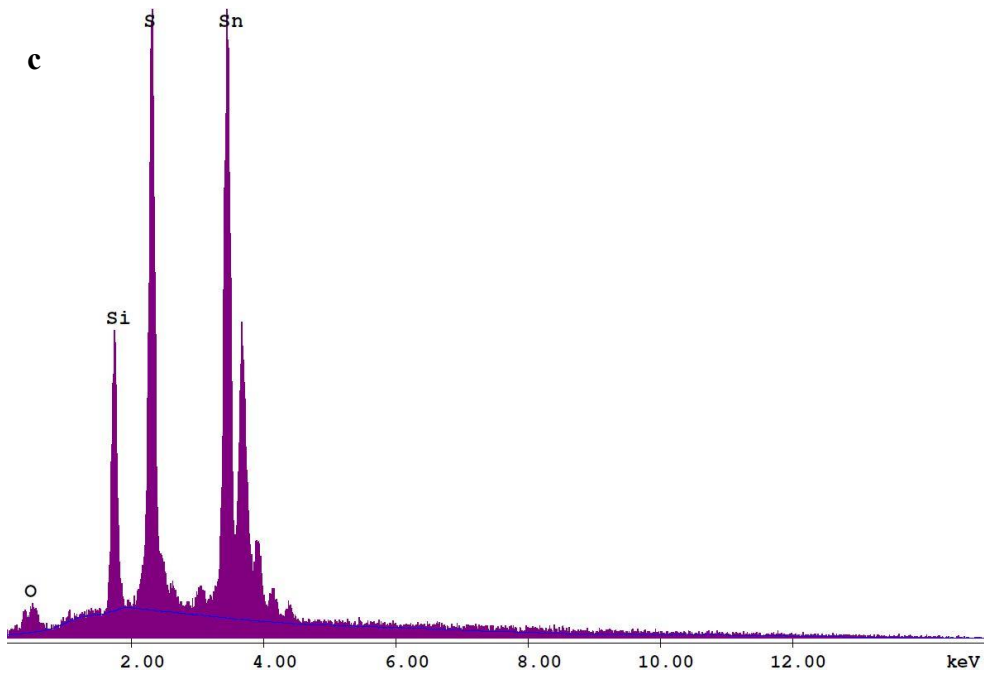
3.1.2 EDAX results

Figure 3.2 shows the EDAX results of these three binary nanoparticles. The substrate of these samples is glass so all the results show silicon and oxygen peaks. The elemental ratio of the metal to sulfur has been used to verify if the binary nanoparticles are the desired ones. In Figure 3.2(a), the ratio of Cu to S is 7:5, which indicates that the sulfide is not 1:1 CuS but Cu_xS ($1 < x < 2$). The copper sulfide is commonly a mixture of Cu_xS and since we only care the elemental ratio in mixture, it is an acceptable result as long as there are only two elements, copper and sulfur, showing up.

As shown in Figure 3.2(b) and 3.2(c), the elemental ratios of metal to sulfide for both the ZnS and SnS are almost 1:1 which indicate that these two binary nanoparticles are the desired metal sulfides.



| Element | Wt % | At % | K-Ratio | Z | A | F |
|---------|--------|--------|---------|--------|--------|--------|
| O K | 2.95 | 8.69 | 0.0107 | 1.1568 | 0.3123 | 1.0016 |
| SiK | 0.66 | 1.10 | 0.0043 | 1.1179 | 0.5894 | 1.0053 |
| S K | 27.43 | 40.39 | 0.2342 | 1.0972 | 0.7780 | 1.0000 |
| ZnK | 68.97 | 49.81 | 0.6493 | 0.9424 | 0.9991 | 1.0000 |
| Total | 100.00 | 100.00 | | | | |



| Element | Wt % | At % | K-Ratio | Z | A | F |
|---------|--------|--------|---------|--------|--------|--------|
| O K | 3.66 | 13.94 | 0.0080 | 1.2410 | 0.1767 | 1.0001 |
| SiK | 6.64 | 14.40 | 0.0567 | 1.2193 | 0.6941 | 1.0088 |
| S K | 18.48 | 35.11 | 0.1832 | 1.1871 | 0.8229 | 1.0147 |
| SnL | 71.22 | 36.55 | 0.6298 | 0.9041 | 0.9781 | 1.0000 |
| Total | 100.00 | 100.00 | | | | |

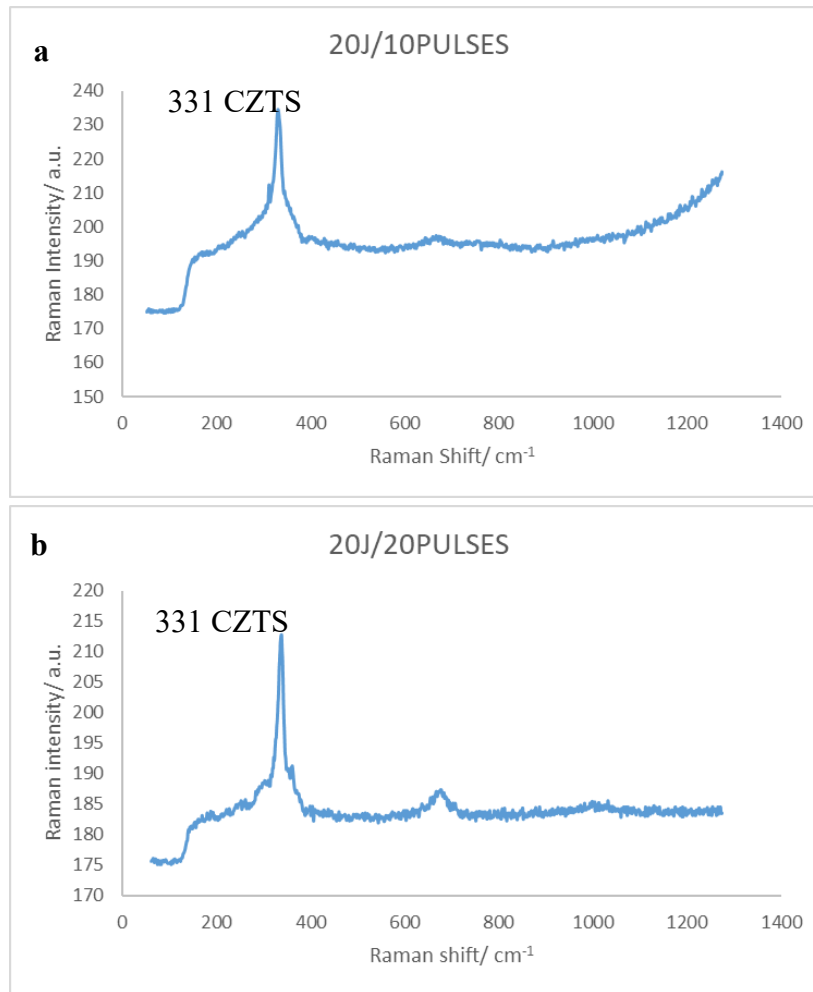
Figure 3.2 EDAX results of a) CuS, b) ZnS, c) SnS

3.2 IPL samples

The best samples in this process are from IPL so characterizations are focus on these samples. For samples from UV curing and Xenon lamp sintering, the XRD does not show the characteristic CZTS peaks so no further study is done on these samples.

Firstly, experiments applying random energy input are performed to identify how much energy input is a reasonable range to sinter CZTS. Raman shift has been used to check the

CZTS characteristic peak. When the energy input is as low as 1 pulse to 5 pulses per sample, there is no obvious peak in the Raman result. When the pulses are increased to 10 pulses, there are obvious CZTS peaks which are located at 331 cm^{-1} . However, as the energy input increases, the impurity also increases. The main impurities are metal sulfides (CuS, ZnS, and SnS) which are either unreacted precursors or decomposed from the CZTS during sintering and CuSnS_3 byproduct, which also can be found during other thermal processes. As a result, the main reaction condition has been set around 20 J per pulse and 10 pulses.



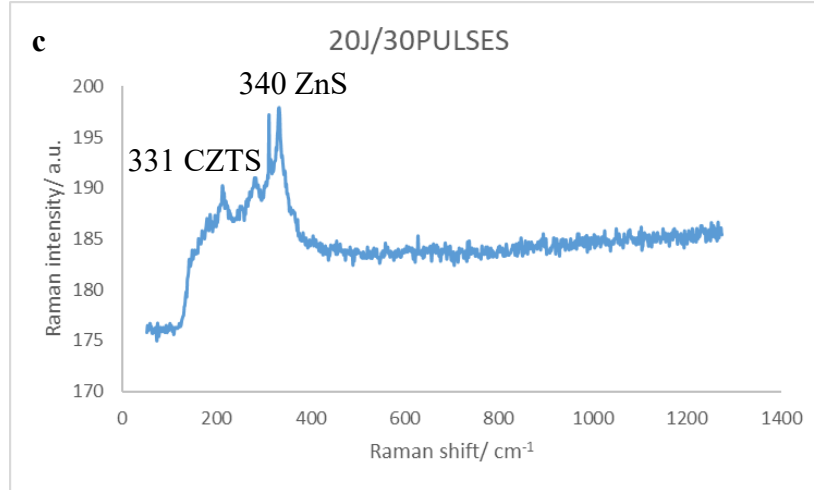


Figure 3.3 Raman results of random tries a) 20 J/pulse × 10 pulses, b) 20 J/pulse × 20 pulses, c) 20 J/pulse × 30 pulses

Table 3.1 shows the reaction condition of the samples. The temperature of sintering should not be above 450°C because CuSnS₃ byproduct will become the majority product if the reaction temperature is above 450°C.^{29, 34-35} As a result, the highest average temperature has been controlled below 450°C.

Table 3.1 Experimental conditions of IPL samples

| Sample number | Sintering energy (J/pulse) | Sintering pulses | Average temperature (°C) |
|---------------|----------------------------|------------------|--------------------------|
| 1 | 10 | 5 | 258.3 |
| 2 | 10 | 10 | 281.8 |
| 3 | 10 | 20 | 351.1 |
| 4 | 16 | 5 | 367.6 |
| 5 | 16 | 10 | 357.5 |
| 6 | 16 | 20 | 417.1 |
| 7 | 20 | 5 | 409.3 |
| 8 | 20 | 10 | 435.6 |
| 9 | 20 | 20 | 444.4 |

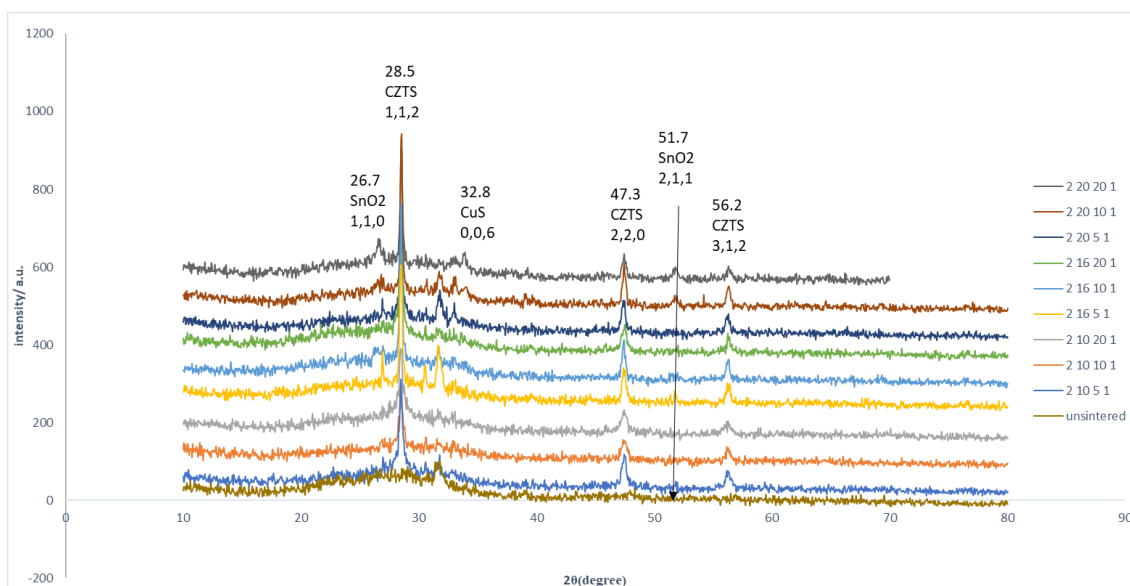


Figure 3.4 XRD results of IPL samples

3.2.1 XRD results of IPL samples

One of the routine methods to determine the crystal structure is XRD. Figure 3.4 shows the XRD results obtained by Bruker Discover 8 diffractometer.

In the XRD results, the unsintered sample only shows CuS peak at $2\theta = 31.8^\circ$. According to Guo *et. al.*, this peak also shows that the material have been well mixed. Besides that, all the sintered sample have the 3 CZTS characteristic peaks at 28.5° (112), 47.3° (220), and 56.2° (312), refer to JCPDS 26-0575.²⁸ When the sintering energy increased, the CZTS characteristic peaks grow as well. Also, the 31.8° peak presents in samples 1-4, which is considered as unreacted precursor. Some impurity peaks such as 26.7° (SnO_2 (110)), 51.7° (SnO_2 (211)) and 32.8° (CuS (006)) are present in samples 7, 8, and 9.

Through the XRD result, it is clear that all the sintered samples have CZTS crystal because all the samples have three main peaks of CZTS. However, as the reaction condition changes, the impurity also changes. When the sintering energy is low, such as in sample 1 to 4, there is also metal sulfide present that shows that the reaction was not complete, some reactant

remains in the thin film after the reaction. When the sintering energy is too high, some CZTS grain will be either oxidized to the metal oxides or decomposed back to metal sulfides, which means the sample is overcooked beyond the target.

3.2.2 UV-Vis result of IPL samples

To identify the band gap of the CZTS film, UV-Visible spectroscopy was used to measure the absorption of the thin film vis Jasco V-670 UV-Vis-NIR spectrometer. The result has been shown in Figure 3.5.

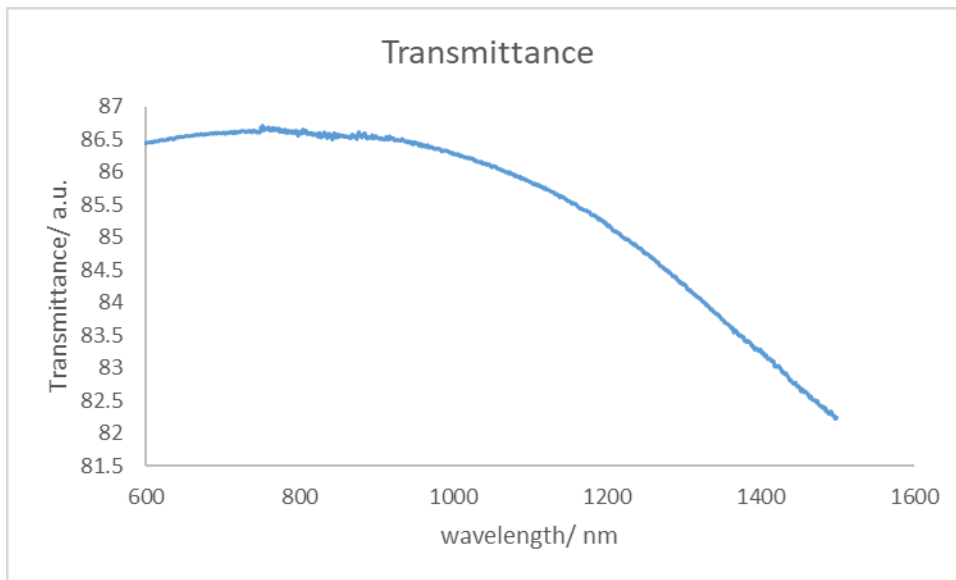


Figure 3.5 UV-Vis result for IPL samples

According to Tauc's article, in semiconductors, the relationship between wavelength and absorption can be used to calculate the bandgap of the material. This relationship can be shown in Tauc's plot. When calculating the $(ah\nu)^2$ (a stands for the absorption, h stands for Plank's constant and ν stands for wavelength) and plot $(ah\nu)^2$ vs wavelength, the intersection of the tangent line and the X-axis is the bandgap of the material. Figure 3.6 shows the Tauc's plot, the bandgap of our CZTS film is 1.41 ± 0.02 eV, which matches the ordinary bandgap of CZTS.

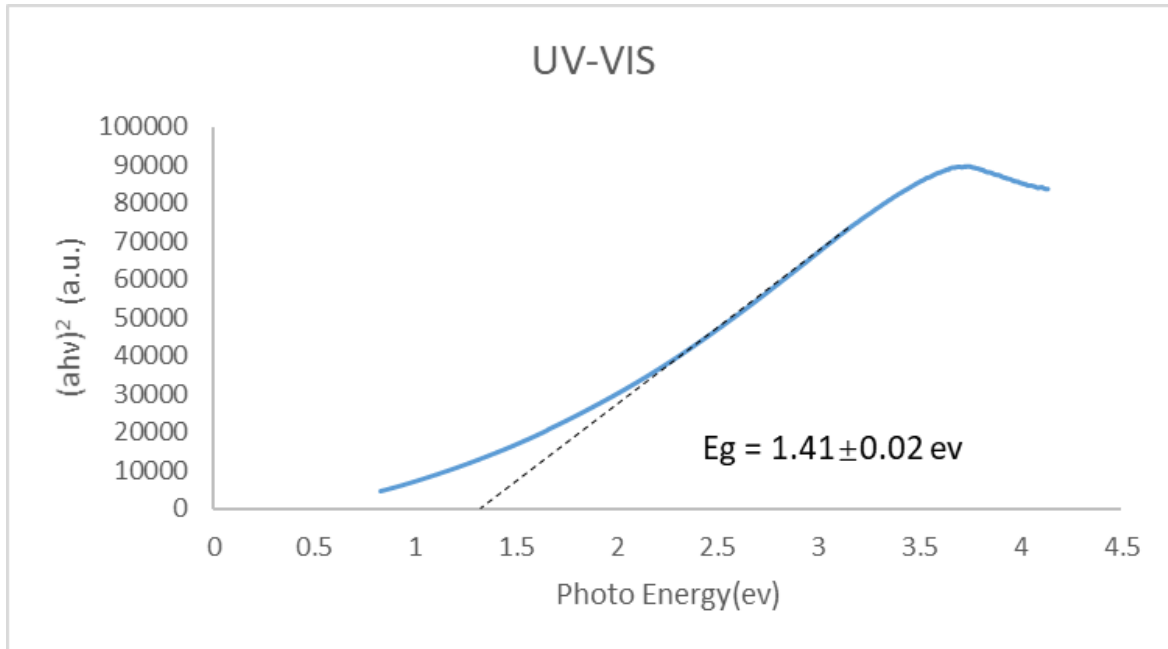


Figure 3.6 Tauc's plot of IPL sample

3.2.3 Raman results of IPL samples

The Raman results of IPL samples varies between each individual sample. In other words, even one sample may have entirely different result at different sampling spot. It could be due to the morphology of the samples not good which lead to every single point of the samples to have a different Raman result. At some points, the Raman results have perfect CZTS peak but some point will show nothing or just some metal sulfide. So here we just report the well-cooked part of the IPL samples. The good thing about Raman is to distinguish ZnS from CZTS because it is very hard to distinguish them in XRD. In XRD, the peaks of CZTS and ZnS are very similar but in Raman, the peaks of CZTS are located at 330 cm^{-1} and 285 cm^{-1} , while the peak of ZnS is located at 340 cm^{-1} .⁴⁰ Thus the Raman result is a strong evidence that the IPL samples contain CZTS which shows in Figure 3.7.

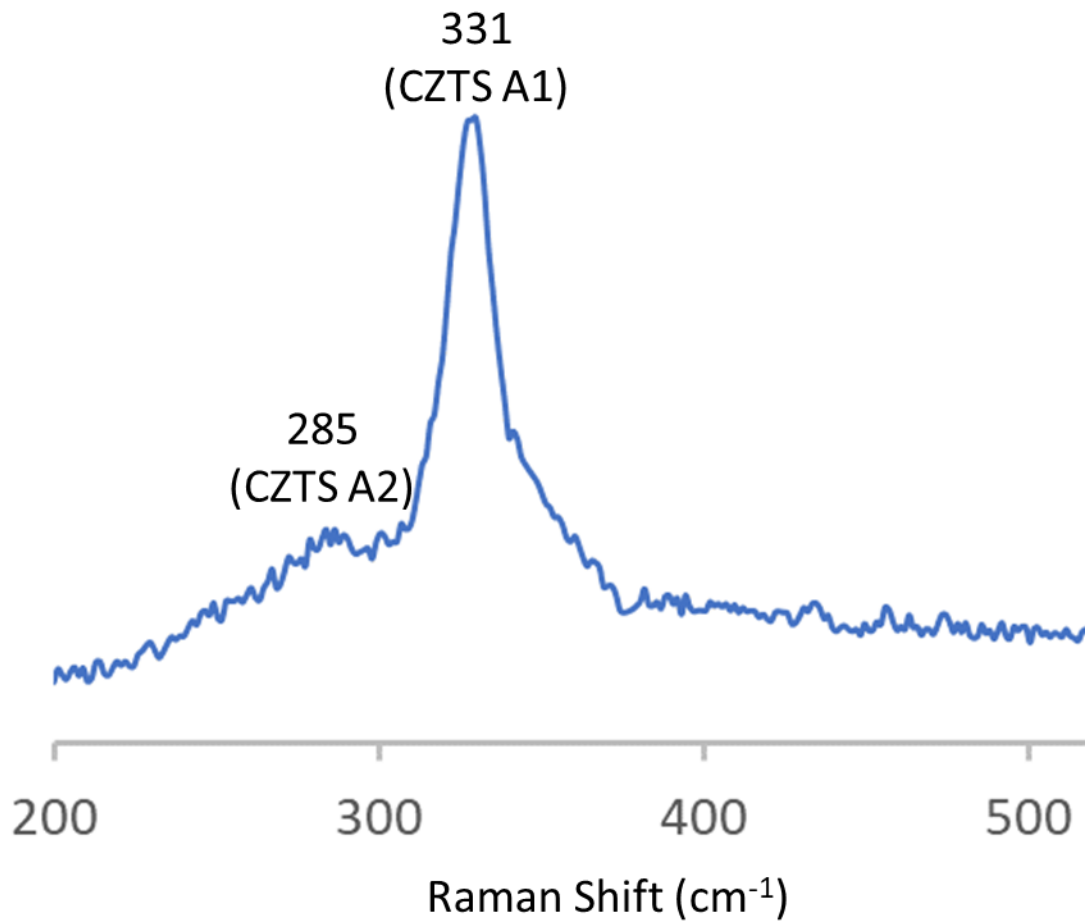


Figure 3.7 Raman result of IPL samples

3.2.4 SEM results of IPL samples

To further research the morphology of the IPL samples, SEM have been introduced to obtain the topview and cross-section images of the IPL samples. Figure 3.9 shows the SEM images of these samples.

Figure 3.9.a shows the cross-sectional view of these samples. All these samples use the same spin coating method so the thickness of these samples is quite similar. The thickness of these samples varies from 1 μm to 2 μm .

Figure 3.9.b and 3.9.c show the low magnification (500 \times to 2,000 \times) top view of the samples. Basically, these samples all have some cracking and bubble-like surface which all

have certain defects on the morphology of the thin film. One possible explanation for the cracking and bubble-like surface is that the cracking is a result of the thermal expansion and the bubble-like surface is due to the evaporation of thiourea. When other kinds of metal sulfide are dispersed in the solution, the thiourea is dissolved in the solution. So, when the thiourea crystallized, they will form far more big crystal than nano size. When thiourea is heated up, it will easily decompose to gas form, which will cause this bubble-like surface especially when thiourea is buried in the thin film. Besides, all the material will expand when been heated and contract when cooled. So, when this whole process happens very fast, the distance between material will be expanded so the crackers will be created.

The rest of the images here are the small-scale view of the IPL samples. All these samples have some amorphous parts (Figure 3.8.e) and crystal parts (Figure 3.8.d). The difference among these samples is that the ratio of the crystal part/amorphous part and the size of the grains. In total, when the sintering energy increases, the crystalline part and the grain size will also increase until the sintering energy has reached 20 joules per pulse and 10 pulses. When the sintering energy is below 16 joules per pulse and 10 pulses, the grain is like Figure 3.8.d that only has small crystalline part and small grain size. Figure 3.8.f shows when the sintering energy increases to 20 joules per pulse and 5 pulses, the crystalline area is larger and grain size is bigger. However, when the sample is overcooked like 20 joules per pulse and 10 pulses, the grain size will become small again as shown in Figure 3.9.h and some crystals melt down (Figure 3.8.g & 3.8.h). The grain size in Figure 3.8.i and 3.8.j is at a scale of 60 nm~100 nm.

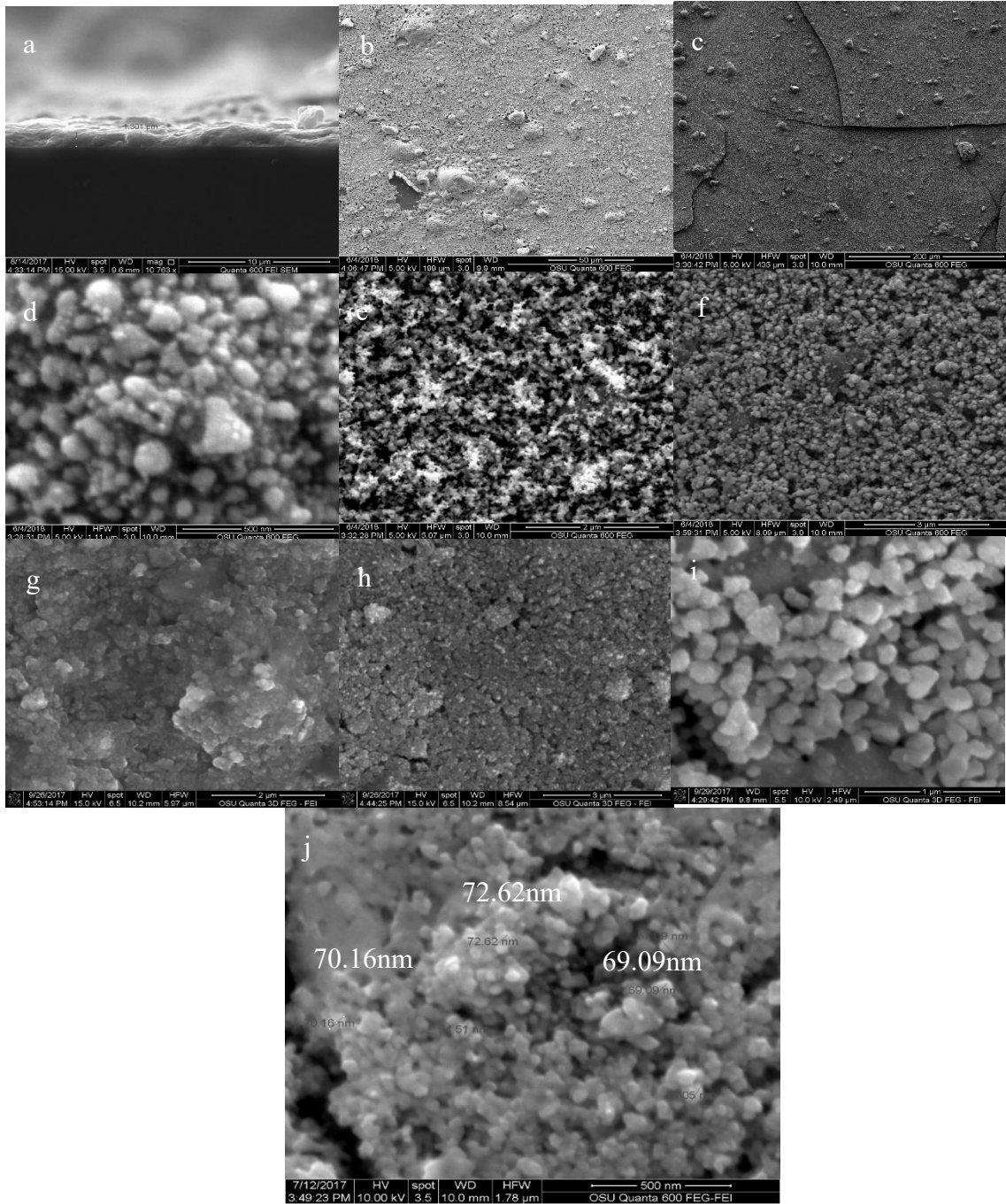


Figure 3.8 SEM of IPL samples: a) cross-sectional image, b) & c) low magnification top views, d) crystalline part, e) amorphous part, f) crystalline part of sample with 20 J & 5 pulses sintering power, g) & h) crystalline part of sample with 20 J & 10 pulses sintering power, i) & j) grain size measurement

3.2.5 TEM result of IPL samples

Additionally, TEM has been used to check the sub-micron structure of CZTS thin film sample. The TEM result has been shown in Figure 3.9. The highest intensity XRD peak for CZTS is 28.5° for (112). According to Bragg's law, $n\lambda = d\sin\theta$. θ stands for the angle, which is 28.5° . Distance of equipment is 0.325×10^{-9} m and the wavelength of incoming X-ray is 2.5×10^{-12} m. According to the calculation, N is 124, which means this distance matches the first peak of CZTS.

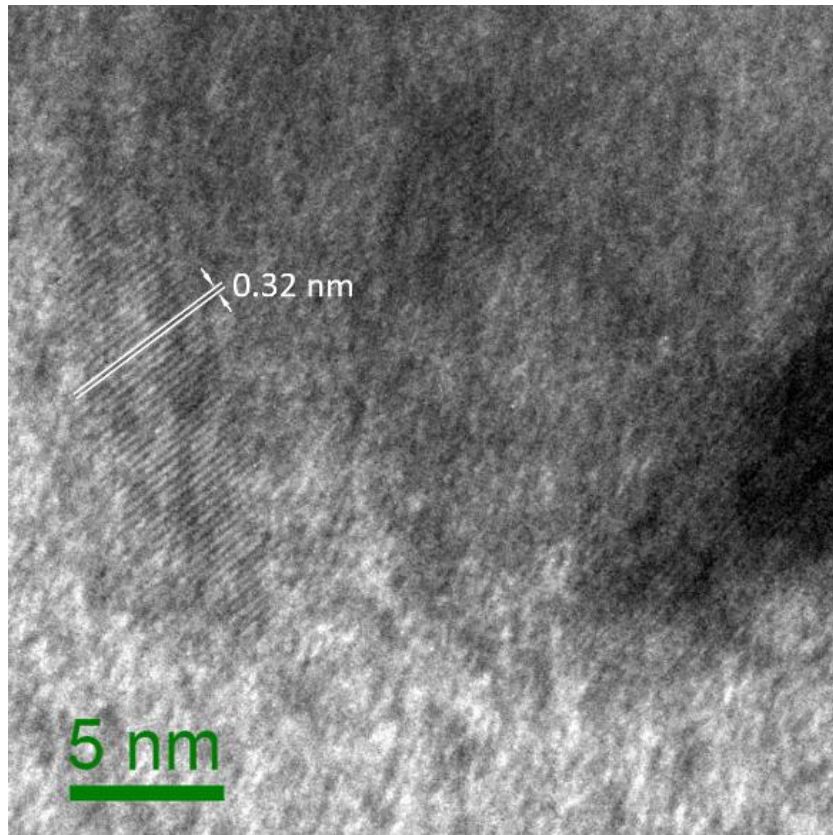


Figure 3.9 TEM result of IPL samples

3.2.6 Hall effect result of IPL samples

Hall effect on room temperature has been measured by HMS 5000. The results are shown in Table 3.2.

Table 3.2 Hall effect results of IPL samples

| sample number | Resistivity ($\Omega \cdot \text{cm}$) | Conductivity ($1/(\Omega \cdot \text{cm})$) | Mobility (cm^2/Vs) | Average Hall coefficient (cm^3/C) |
|---------------|--|---|--------------------------------------|---|
| 1 | 0.35 | 2.87 | 3.73 | 1.30 |
| 2 | 0.040 | 25.26 | 8.56 | 0.34 |
| 3 | 0.28 | 3.60 | 4.34 | 1.21 |
| 4 | 0.026 | 38.76 | 7.34 | 0.19 |
| 5 | 0.020 | 51.24 | 4.77 | 0.093 |
| 6 | 0.024 | 40.96 | 0.99 | 0.024 |
| 7 | 0.065 | 15.35 | 0.37 | 0.024 |
| 8 | 0.088 | 11.39 | 123.20 | 10.81 |
| 9 | 0.041 | 24.15 | 333.50 | 13.81 |

It is shown that all the samples have similar resistivity, conductivity and average hall coefficient. However, when the sintering energy is increased to 20 joules per pulse and 10 pulses, the mobility shows a great increase. A possible reason is when the input energy has reached a relatively high level, the crystallized CZTS will be decomposed again and some of them will form oxides. However, there is no confirmed evidence that can prove this.

3.2.7 Methylene blue degradation result

Because the time is limited, two samples with 16 joules per pulse/20 pulses (CZTS in Table. 3.2) and 20 joules per pulse/ 10 pulses (Overcooked CZTS in Figure 3.12) have been used to demonstrate the photocatalysis degradation rate of methylene blue. The MB concentration change is shown in Figure 3.10.

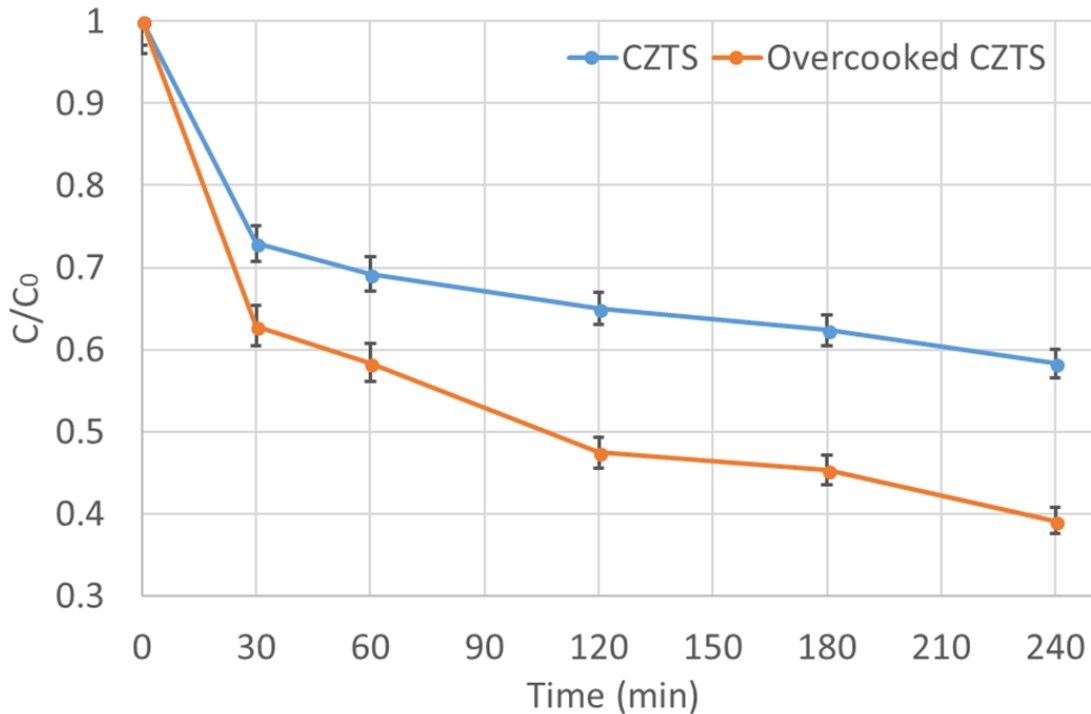


Figure 3.10 Concentration change for Methylene under the light

The result shows that the degradation of methylene blue is very fast at the first 30 mins and slow down to a nearly constant speed after that. Also, the CZTS samples have just CZTS while the overcooked CZTS have both CZTS and impurity (metal sulfide and metal oxide), the efficiency of overcooked CZTS is much higher than the pure CZTS.

One possible reason for the degradation speed change is that the reaction rate is limited by the concentration of dissolved oxygen in water. As shown in Chapter 2, 3.1, one important step of the degradation is converting dissolved oxygen to $O_2^{\cdot -}$ radical. Initially the oxygen is saturated in water so the reaction rate is relatively high at first. However, as the reaction goes on, the dissolving speed of oxygen is much lower than the consumption, so the reaction speed after 30 mins is limited by the speed of oxygen dissolved in water.

Besides, the CZTS and oxide may form a p-n heterojunction as shown in Figure 3.11. With pure CZTS thin film, some of the photon generated electron-hole pair will recombine and cannot further generate radicals. When the film consists of CZTS and oxide, they will form a p-n junction and the holes and electrons can be further separated which can restrict the

recombination of the material. Thus, more holes and electrons can take place in the reaction, resulting in higher reaction rate.

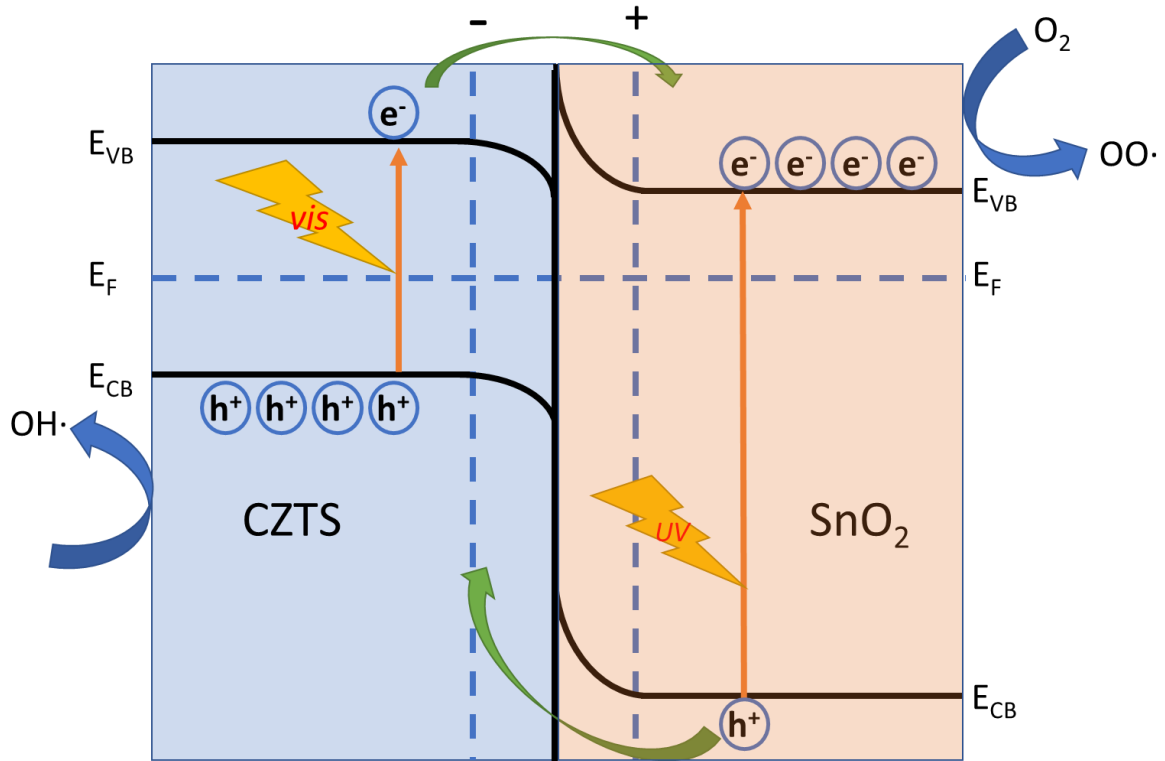


Figure 3.11 Schematic diagram showing the energy band structure and electron-hole pair separation in the CZTS-SnO₂ heterojunction.

Chapter 4 Conclusion and future plan

From spin coating method and IPL sintering, thin CZTS film has been made in very short time and tested through methylene blue degradation experiment. Since the morphology is not good. In the future, a printing process can be introduced to improve the morphology and the film can be made sans thiourea but in the H₂S atmosphere. Also, a continuous flow cell for photocatalysis reaction which can introduce oxygen into the water will help the research on the efficiency of the thin film in the methylene blue degradation.

In conclusion, a roll to roll system may be built and the whole production can be done in very short time in the future.

Reference:

1. BP BP *Statistical Review of World Energy*; 2018.
2. Perea, A.; Honeyman, C.; Smith, C.; Mond, A.; Shiao, M.; Jones, J.; Moskowitz, S.; Gallagher, B.; Davis, M.; Rumery, S.; Holm, A.; O'Brien, K.; Baca, J. *US Solar Market Insight Executive Summary*; 2018.
3. Administration, U. S. E. i., *Electric Power Monthly with Data for April 2018*.
4. Yamaguchi, M.; Lee, K.-H.; Araki, K.; Kojima, N., A review of recent progress in heterogeneous silicon tandem solar cells. *Journal of Physics D: Applied Physics* **2018**, *51* (13), 133002.
5. Green, M. A., The path to 25% silicon solar cell efficiency: History of silicon cell evolution. *Progress in Photovoltaics: Research and Applications* **2009**, *17* (3), 183-189.
6. Green, M. A.; Hishikawa, Y.; Dunlop, E. D.; Levi, D. H.; Hohl-Ebinger, J.; Ho-Baillie, A. W. Y., Solar cell efficiency tables (version 51). *Progress in Photovoltaics: Research and Applications* **2018**, *26* (1), 3-12.
7. Kato, T., Cu(In,Ga)(Se,S)₂ solar cell research in Solar Frontier: Progress and current status. *Japanese Journal of Applied Physics* **2017**, *56* (4S), 04CA02.
8. Survey, U. S. G., *Mineral Commodity Summaries 2017*.
9. Ramasamy, K.; Malik, M. A.; O'Brien, P., Routes to copper zinc tin sulfide Cu₂ZnSnS₄ a potential material for solar cells. *Chem Commun (Camb)* **2012**, *48* (46), 5703-14.
10. Wang, W.; Winkler, M. T.; Gunawan, O.; Gokmen, T.; Todorov, T. K.; Zhu, Y.; Mitzi, D. B., Device Characteristics of CZTSSe Thin-Film Solar Cells with 12.6% Efficiency. *Advanced Energy Materials* **2014**, *4* (7), 1301465.
11. Haight, R.; Gershon, T.; Gunawan, O.; Antunez, P.; Bishop, D.; Lee, Y. S.; Gokmen, T.; Sardashti, K.; Chagarov, E.; Kummel, A., Industrial perspectives on earth abundant, multinary thin film photovoltaics. *Semiconductor Science and Technology* **2017**, *32* (3), 033004.
12. Byungha Shin, O. G., Yu Zhu, Nestor A. Bojarczuk, S. Jay Chey and Supratik Guha*, Thin film solar cell with 8.4% power conversion efficiency using an earth-abundant Cu₂ZnSnS₄ absorber.
13. Gour, K. S.; Yadav, A. K.; Singh, O. P.; Singh, V. N., Na incorporated improved properties of Cu₂ZnSnS₄ (CZTS) thin film by DC sputtering. *Vacuum* **2018**, *154*, 148-153.
14. Lin, Y.-P.; Chi, Y.-F.; Hsieh, T.-E.; Chen, Y.-C.; Huang, K.-P., Preparation of Cu₂ZnSnS₄ (CZTS) sputtering target and its application to the fabrication of CZTS thin-film solar cells. *Journal of Alloys and Compounds* **2016**, *654*, 498-508.
15. Singh, O. P.; Parmar, R.; Gour, K. S.; Dalai, M. K.; Tawale, J.; Singh, S. P.; Singh, V. N., Synthesis and characterization of petal type CZTS by stacked layer reactive sputtering. *Superlattices and Microstructures* **2015**, *88*, 281-286.
16. Espindola-Rodriguez, M.; Placidi, M.; Vigil-Galán, O.; Izquierdo-Roca, V.; Fontané, X.; Fairbrother, A.; Sylla, D.; Saucedo, E.; Pérez-Rodríguez, A., Compositional optimization of photovoltaic grade Cu₂ZnSnS₄ films grown by pneumatic spray pyrolysis. *Thin Solid Films* **2013**, *535*, 67-72.
17. Rajeshmon, V. G.; Poornima, N.; Sudha Kartha, C.; Vijayakumar, K. P., Modification of the optoelectronic properties of sprayed In₂S₃ thin films by indium diffusion for application as buffer layer in CZTS based solar cell. *Journal of Alloys and Compounds* **2013**, *553*, 239-244.

18. Bhosale, S. M.; Suryawanshi, M. P.; Gaikwad, M. A.; Bhosale, P. N.; Kim, J. H.; Moholkar, A. V., Influence of growth temperatures on the properties of photoactive CZTS thin films using a spray pyrolysis technique. *Materials Letters* **2014**, *129*, 153-155.
19. Singh, M.; Jiu, J.; Sugahara, T.; Suganuma, K., Photonic sintering of thin film prepared by dodecylamine capped $\text{CuIn}_x\text{Ga}_{1-x}\text{Se}_2$ nanoparticles for printed photovoltaics. *Thin Solid Films* **2014**, *565*, 11-18.
20. Vigil-Galán, O.; Courel, M.; Andrade-Arvizu, J. A.; Sánchez, Y.; Espíndola-Rodríguez, M.; Saucedo, E.; Seuret-Jiménez, D.; Titsworth, M., Route towards low cost-high efficiency second generation solar cells: current status and perspectives. *Journal of Materials Science: Materials in Electronics* **2014**, *26* (8), 5562-5573.
21. Farinella, M.; Inguanta, R.; Spanò, T.; Livreri, P.; Piazza, S.; Sunseri, C., Electrochemical Deposition of CZTS Thin Films on Flexible Substrate. *Energy Procedia* **2014**, *44*, 105-110.
22. Mkawi, E. M.; Ibrahim, K.; Ali, M. K. M.; Farrukh, M. A.; Allam, N. K., Influence of precursor thin films stacking order on the properties of $\text{Cu}_2\text{ZnSnS}_4$ thin films fabricated by electrochemical deposition method. *Superlattices and Microstructures* **2014**, *76*, 339-348.
23. Lee, K. D.; Seo, S.-W.; Lee, D.-K.; Kim, H.; Jeong, J.-h.; Ko, M. J.; Kim, B.; Kim, D. H.; Kim, J. Y., Preparation of $\text{Cu}_2\text{ZnSnS}_4$ thin films via electrochemical deposition and rapid thermal annealing. *Thin Solid Films* **2013**, *546*, 294-298.
24. Singh, M.; Jiu, J.; Suganuma, K.; Kim, J., Non-toxic precursor solution route for fabrication of CZTS solar cell based on all layers solution processed. *Journal of Alloys and Compounds* **2015**, *646*, 497-502.
25. Mokurala, K.; Mallick, S.; Bhargava, P., Low Temperature Synthesis and Characterization of $\text{Cu}_2\text{ZnSnS}_4$ (CZTS) Nanoparticle by Solution Based Solid State Reaction Method. *Energy Procedia* **2014**, *57*, 73-78.
26. Huang, Y.; Li, G.; Fan, Q.; Zhang, M.; Lan, Q.; Fan, X.; Zhou, Z.; Zhang, C., Facile solution deposition of $\text{Cu}_2\text{ZnSnS}_4$ (CZTS) nano-worm films on FTO substrates and its photoelectrochemical property. *Applied Surface Science* **2016**, *364*, 148-155.
27. Kim, K.-J.; Pan, C.; Bansal, S.; Malhotra, R.; Kim, D.-H.; Chang, C.-H., Scalably synthesized environmentally benign, aqueous-based binary nanoparticle inks for $\text{Cu}_2\text{ZnSn}(\text{S},\text{Se})_4$ photovoltaic cells achieving over 9% efficiency. *Sustainable Energy & Fuels* **2017**, *1* (2), 267-274.
28. Guo, Q.; Caspar, J. V.; Roelofs, K. E.; Subramoney, S.; Rosenfeld, H. D., Formation of Cu-Rich and Sn-Poor CZTSSe via $\text{Cu}_3\text{Sn}(\text{S},\text{Se})_4\text{-ZnS}$ Solid-Solution as the Intermediate. *Chemistry of Materials* **2014**, *26* (19), 5664-5674.
29. Collord, A. D.; Hillhouse, H. W., Composition Control and Formation Pathway of CZTS and CZTGS Nanocrystal Inks for Kesterite Solar Cells. *Chemistry of Materials* **2015**, *27* (5), 1855-1862.
30. Shin, S. W.; Han, J. H.; Park, C. Y.; Kim, S.-R.; Park, Y. C.; Agawane, G. L.; Moholkar, A. V.; Yun, J. H.; Jeong, C. H.; Lee, J. Y.; Kim, J. H., A facile and low cost synthesis of earth abundant element $\text{Cu}_2\text{ZnSnS}_4$ (CZTS) nanocrystals: Effect of Cu concentrations. *Journal of Alloys and Compounds* **2012**, *541*, 192-197.
31. Wang, W.; Shen, H.; He, X.; Li, J., Effects of sulfur sources on properties of $\text{Cu}_2\text{ZnSnS}_4$ nanoparticles. *Journal of Nanoparticle Research* **2014**, *16* (6).
32. Knutson, T. R.; Hanson, P. J.; Aydil, E. S.; Penn, R. L., Synthesis of $\text{Cu}_2\text{ZnSnS}_4$ thin films directly onto conductive substrates via selective thermolysis using microwave energy. *Chem Commun (Camb)* **2014**, *50* (44), 5902-4.

33. Saravana Kumar, R.; Ryu, B. D.; Chandramohan, S.; Seol, J. K.; Lee, S.-K.; Hong, C.-H., Rapid synthesis of sphere-like Cu₂ZnSnS₄ microparticles by microwave irradiation. *Materials Letters* **2012**, *86*, 174-177.
34. Nguyen, D.-C.; Ito, S.; Dung, D. V. A., Effects of annealing conditions on crystallization of the CZTS absorber and photovoltaic properties of Cu(Zn,Sn)(S,Se)₂ solar cells. *Journal of Alloys and Compounds* **2015**, *632*, 676-680.
35. Prabeesh, P.; Selvam, I. P.; Potty, S. N., Effect of annealing temperature on a single step processed Cu₂ZnSnS₄ thin film via solution method. *Thin Solid Films* **2016**, *606*, 94-98.
36. Buller, S.; Strunk, J., Nanostructure in energy conversion. *Journal of Energy Chemistry* **2016**, *25* (2), 171-190.
37. Yang, W.; Duan, H. S.; Cha, K. C.; Hsu, C. J.; Hsu, W. C.; Zhou, H.; Bob, B.; Yang, Y., Molecular solution approach to synthesize electronic quality Cu₂ZnSnS₄ thin films. *J Am Chem Soc* **2013**, *135* (18), 6915-20.
38. Guan, H.; Shen, H.; Raza, A., Solvothermal Synthesis of p-type Cu₂ZnSnS₄-Based Nanocrystals and Photocatalytic Properties for Degradation of Methylene Blue. *Catalysis Letters* **2017**, *147* (7), 1844-1850.
39. Hurma, T.; Kose, S., XRD Raman analysis and optical properties of CuS nanostructured film. *Optik - International Journal for Light and Electron Optics* **2016**, *127* (15), 6000-6006.
40. Seboui, Z.; Gassoumi, A.; Cuminal, Y.; Kamoun-Turki, N., Effect of annealing process on the properties of Cu₂ZnSnS₄ thin films. *Superlattices and Microstructures* **2014**, *75*, 586-592.